Thesis for the Degree of Licentiate of Engineering

Facilitating Electric Passenger Transport Systems Integrating Renewable Energy Sources

Omkar Parishwad

CHALMERS

Department of Architecture and Civil Engineering
Chalmers University of Technology
Gothenburg, Sweden, 2025

Facilitating Electric Passenger Transport Systems Integrating Renewable Energy Sources

Omkar Parishwad

Supervisor
Dr. Kun Gao, Docent
Urban Mobility Research Area,
Division of Geology and Geotechnics
Department of Architecture and Civil Engineering
Chalmers University of Technology, Sweden

Co-supervisors
Dr. Arsalan Najafi
Dr. Jelena Andric
Urban Mobility Research Area,
Division of Geology and Geotechnics
Department of Architecture and Civil Engineering
Chalmers University of Technology, Sweden

Technical Report No. ACE 2025:5

Urban Mobility Research Area
Division of Geology and Geotechnics
Department of Architecture and Civil Engineering
Chalmers University of Technology
Gothenburg, SE 412 96, Sweden
Phone: +46(0)31 772 1000

Chalmers Reproservice
Gothenburg, Sweden 2025.

Cover: Image created using a prompt in Microsoft Copilot.

Facilitating Electric Passenger Transport Systems Integrating Renewable Energy Sources

Omkar Parishwad
Department of Architecture and Civil Engineering
Chalmers University of Technology

Abstract

Transport electrification driven by net-zero emission targets in the transport sector requires accurate prediction of charging demand and cost effective deployment of charging and energy infrastructure. This thesis begins with a comprehensive review of infrastructure and energy supply for transport electrification, with emphasis on near-term charging demand prediction, the integration of renewable energy with charging infrastructure, and system-level impacts.

Addressing identified research gaps, the first study develops an integrated agent-based modeling framework to generate spatiotemporal charging demand profiles. The framework jointly accounts for cost-aware charging behavior, daily activity chains, and route and mode choice, while incorporating multiple charger types, dynamic time-of-use tariffs, and probabilistic adaptive smart-charging behavior that allows users to shift charging to reduce costs while mitigating range anxiety.

Building on the near-future charging demand outputs, the second study develops a large-scale optimization framework for the deployment of multi-class public chargers, co-located photovoltaic systems, and battery energy storage (BESS). The framework jointly optimizes charger placement, PV sizing, BESS scheduling, and user incentives for short-distance spatial demand redirection, while accounting for land-use constraints, seasonal PV capacity factors, and time-of-use tariffs.

The developed approaches are demonstrated in a real-world case study of Gothenburg using multisource data. System benefits are assessed across economic, operational, and environmental dimensions. The results provide quantitative evidence on how user charging behavior and smart charging influence spatiotemporal demand, and how the integration of renewable energies with BESS and incentive-based demand management can jointly enable cost-effective and sustainable charging and energy supply for electric passenger transport.

Keywords: Integrated modeling and optimization; Charging demand forecasting; Charging preferences; Diverse user behavior; Charging infrastructure deployment; Renewable energy; Battery storage systems.

List of Publications

Appended publications

This thesis is based on the following publications:

[**Paper I**] **O. Parishwad**, A. Najafi, X. Liu, K. Gao (2025), *The Role of Renewable Energy to Promote Future Electric Transport and Power Systems*
The Routledge Handbook of Sustainable Urban Transport, pp. 361–373,; doi:10.4324/9781003425489-30.

[**Paper II**] **O. Parishwad**, K. Gao, A. Najafi, *Integrated and agent-based charging demand estimation considering cost-aware and adaptive charging behavior*
Transportation Research Part D: Transport and Environment (under review).

[**Paper III**] **O. Parishwad**, K. Gao, A. Najafi, *Joint optimization of charging infrastructure and renewable energies with battery storage considering user redirection incentives.*
Finished work to be submitted.

Other relevant publications

[**a**] A. Najafi, K. Gao, **O. Parishwad**, G. Tsaousoglou, S. Jin, W. Yi (2025), *Integrated optimization of charging infrastructure, electric bus scheduling and energy systems*
Transportation Research Part D: Transport and Environment, Vol. 141, 104664. doi:10.1016/j.trd.2025.104664.

[**b**] A. Najafi, K. Gao, H. Wang, M. Jasinski, **O. Parishwad**, S. Cui, X. Liu (2025), *Joint charging scheduling of electric buses and active power flexibility integration*
Transportation Research Part E: Logistics and Transportation Review, Article 104038. doi:10.1016/j.tre.2025.104038.

[**c**] **O. Parishwad**, K. Gao, A. Najafi, *Modeling e-scooter sharing demand and its influencing factors: A spatial machine learning approach*
Journal of Transport Geography (under review). doi:10.2139/ssrn.5232197.

Acknowledgement

This thesis is a part of my ongoing work carried out from January 2023 to August 2025 at the Department of Architecture and Civil Engineering (ACE), Chalmers University of Technology.

First and foremost, I express my deepest gratitude to my supervisor, **Kun Gao** ("*Guru Brahma, Guru Vishnu..*"). Your clear guidance, constructive feedback, and steady support have profoundly shaped both this research and my development as a scholar. Your genius has inspired me to evolve into a rigorous, responsible, and passionate researcher. I am also profoundly thankful to my co-supervisors, **Arsalan Najafi** and **Jelena Andric**. Your deep subject expertise and many helpful discussions, particularly in electrical systems and optimization, were invaluable in refining my methodological approaches. More than that, your warmth and kindness has made this journey not only enlightening but enjoyable. A special thank you goes to **Lars Rosen**, who taught me to balance my research and life. Whose steadfast confidence in me and timely motivation helped me maintain focus and composure during the more challenging phases of my PhD at Chalmers. I have greatly benefited from the warm collegial environment at ACE and from discussions with colleagues in the Urban Mobility Research Area at Chalmers.

This work was supported by the *Area of Advance (AoA) Transport* at Chalmers and, in part, by *JPI Urban Europe* and the *Swedish Energy Agency (Energimyndigheten)* under the *e-MATS project (P2023-00029)*. The views expressed are those of the author and do not necessarily reflect those of the sponsors.

On a deeply personal note, I wish to honor the memory of my father, the late professor **G.V. Parishwad**. A lifelong academician and devoted researcher, whose pursuit of knowledge laid the foundation for my own. I followed in his footsteps at Chalmers, driven by the same curiosity and passion. I remember him daily with profound fondness and a sense of longing.
To all who have supported me, colleagues, friends, and family, thank you for your encouragement, kindness, and belief in my work. This thesis is as much yours as it is mine...

Omkar Parishwad
August 2025

Contents

Acronyms

EV	Electric Vehicle
CPO	Charging Point Operator
RES	Renewable Energy Sources
PV	Photovoltaic
BESS	Battery Energy Storage System
SoC	State-of-Charge
ToU	Time-of-Use
GTFS	General Transit Feed Specification
LULC	Land-Use and Land-Cover
OSM	Open StreetMap
PDS	Power Distribution System
V2G	Vehicle to Grid
ABM	Agent-Based Modeling
CapEx	Capital Expenditure
SEK	Swedish krona
MILP	Mixed-Integer Linear Programming
MATSim	Multi-Agent Transport Simulation

Chapter 1

Introduction

The electrification of urban passenger transport is accelerating, driven by binding decarbonisation targets and rapid advances in vehicle and charging technologies. The global Electric Vehicle (EV) fleet increased from 26 million in 2022 to 40 million in 2023 and is projected to approach 60 million by 2025 (Cavalcante et al., 2024). In Europe, EV market share is expected to rise from 18 % in 2023 to 25 % in 2025 and exceed 60 % by 2030 (Zaino et al., 2024; Jung et al., 2023). Sweden aims to reach net-zero greenhouse gas emissions by 2045 under its national Climate Act, while EU policy frameworks mandate climate neutrality by 2050, with EVs identified as a central component of the transition (Rodrigues et al., 2023).

High penetration of EVs brings significant charging and energy infrastructure challenges, which are both technical and behavioral, and must be captured to guide infrastructure planning. Uncoordinated charging can increase local peak demand by up to 35 %, risking transformer overloads, voltage instability, and costly reinforcements in the Power Distribution System (PDS) (Alvarez Guerrero et al., 2022; Ibrahim et al., 2024). Public charging infrastructure deployment is lagging. Only 150 000 new chargers were installed in 2023, compared with the 410 000 with over 1.2 million units per year needed to meet 2030 targets (Karuppiah et al., 2024). Projections indicate that accommodating an additional 75 million EVs by 2030 in Europe could require over € 6.7 trillion in grid upgrades by 2050 (Christensen et al., 2024). Integrating on-site Renewable Energy Sources (RES), particularly Photovoltaic (PV) generation with co-located Battery Energy Storage System (BESS) (Stecca et al., 2022), and applying smart charging control strategies (Singh et al., 2022), offers a viable mitigation pathway. Case studies show that co-located PV–BESS can reduce peak grid imports by about 18 % (Thunuguntla et al., 2024), while Time-of-Use (ToU) tariffs and other adaptive charging strategies can shift at least 20 % of load to off-peak periods (Zhong et al., 2024b). Such measures improve grid resilience, reduce operational costs, and increase the utilization of locally generated renewable electricity (Dey et al., 2024).

Accurate prediction of future charging demand is vital for charging infrastructure deployment, grid management, and policymaking (Kim and Kim, 2021). EVs alone are projected to account for 6–8% of global electricity demand by 2035, underlining the urgency of robust demand estimation methods that extend beyond static averages to behavior-sensitive models (Rietmann et al., 2020). Forecasting remains challenging due to heterogeneous travel patterns, charging behaviors across locations (home, work, public), vehicle specifications, and user preferences. These behaviors are further shaped by external factors such as ToU pricing and smart charging, as spatiotemporal charging costs strongly influence when, where, and how users charge. Despite methodological progress, significant gaps persist. Many models rely on static or simplified assumptions, failing to capture the probabilistic, spatiotemporal, and cost-sensitive nature of charging decisions (Adenaw and Lienkamp, 2021; Yi et al., 2023; Wu et al., 2023). Although sensitivity to dynamic pricing is well documented (Visaria et al., 2022; Ensslen et al., 2018), it is often underrepresented in large-scale agent-based simulations. Some studies incorporate strategies such as plan-ahead and event-triggered charging, but integrated models that jointly account for daily activity chains, dynamic pricing, smart charging, and users' travel and charging preferences remain scarce. Current approaches often separate travel behavior modeling from charging demand estimation, limiting the ability to capture interdependencies between travel and charging behavior (He et al., 2022; Kim and Kim, 2021). These shortcomings constrain realistic emulation of charging patterns and undermine spatiotemporal demand estimation critical for infrastructure and energy planning.

Despite ambitious policy targets, Europe installs only about one-fifth of the public charging points required annually to meet regulatory and projected demand, highlighting a significant infrastructure deficit (Cui and Zhao, 2024; European Commission. Joint Research Centre., 2023). This shortfall emphasizes the need for planning strategies that optimize not just charger numbers, but also their spatial allocation and operational integration. Existing research has advanced charger siting, PV sizing, and BESS deployment, yet typically treats these dimensions in isolation or limited combinations. To date, no unified optimization framework simultaneously addresses multi-class charger placement, PV and BESS deployment, and optimal BESS scheduling. Similarly, while demand-side management and spatial demand redirection have been studied independently, integrating driver acceptance–based incentives into infrastructure and PV–BESS planning to mitigate localized peaks remains unexplored. Moreover, current models often neglect practical constraints such as land-use and parking limitations, PV installation bounds, dynamic ToU tariffs, and the spatiotemporal interplay of charging demand with renewable generation (Sayarshad, 2024; Ji et al., 2024). In summary, the dual challenge lies in accurately forecasting behavior sensitive charging demand and in strategically deploying charging and energy infrastructure under real-world spatial, temporal, and economic constraints. Addressing these gaps motivates the methodological developments in this thesis, with demand modeling and infrastructure optimization to support sustainable transport electrification.

Scope and contributions

Building on the research gaps and motivations outlined above, this thesis is initiated through an extensive literature review (Paper I) to assess the current state of knowledge on transport electrification, focusing on near-future charging demand prediction, impacts on the PDS, and the prospects for integrating RES with charging infrastructure. The review, elaborated in Chapter 2, identifies two primary research gaps. First, accurate estimation of future charging demand for passenger transport requires an integrated and scalable spatiotemporal modeling approach that captures heterogeneous charging behaviors and the influence of dynamic pricing or smart charging technologies, with consideration of daily activity travel patterns, route, and mode choice behaviors. This motivates us to conduct the first research (elaborated in Paper II) to develop an integrated agent-based framework to estimate future spatiotemporal EV charging demand. The framework captures users' charging decisions by linking daily travel behavior (including activity chains, mode, and route choices) with cost-minimizing responses to heterogeneous charging costs of different charger types, ToU electricity pricing, and adaptive smart charging.

Second, the review further synthesizes empirical evidence on how rising EV penetration stresses the PDS, including voltage sags, thermal overloads, and reduced reliability, and catalogs mitigation strategies such as smart grid controls, distributed storage, and RES coupling to improve capacity and stability. Notably, limited work has assessed how co-located PV and BESS can mitigate peak loads under behavior sensitive demand management via user redirection. This motivates us to conduct the second research elaborated in Paper III about a holistic framework to co-optimize multi-class charger infrastructure, PV, and BESS deployment, with co-optimization of BESS discharging and charging scheduling and behaviorally informed user redirection for demand management.

Integrated and agent-based charging demand prediction considering cost-aware and adaptive charging behavior (Paper II):

This study develops an integrated agent-based framework to estimate future spatiotemporal EV charging demand. The framework captures users' charging decisions by linking daily travel behavior (including activity chains, mode, and route choices) with cost-minimizing responses to ToU electricity pricing. It accounts for heterogeneous charging costs across charger types and incorporates smart charging strategies. A central contribution is a probabilistic and adaptive smart charging module that enables users to reschedule charging within plugged-in windows to exploit ToU price variations. Embedded within an extended Multi-Agent Transport Simulation (MATSim) scoring function, the module jointly models mode choice, route choice, and charging behavior, thereby capturing realistic user trade-offs often overlooked in existing models. Agents adjust charging timing and location within their activity windows to minimize cost and maintain sufficient State-of-Charge (SoC), with heterogeneity modeled through configurable awareness and coincidence factors. This generates realistic and spatiotemporal varying demand profiles.

Joint optimization of charging infrastructure and RES with BESS considering user redirection incentives (Paper III):

This study develops a holistic framework for the co-optimization of multi-class charger infrastructure, PV deployment, and BESS integration. The framework incorporates dynamic BESS scheduling that synchronizes charging and discharging with PV generation profiles and ToU electricity tariffs, thereby enhancing system flexibility and maximizing arbitrage opportunities. In addition, it introduces a behaviorally informed user-redirection mechanism that embeds distance- and time-based rebate incentives to mitigate localized peak loads by steering demand toward underutilized and RES-rich charging sites. The framework is validated through a real-world case study leveraging multi-source big data to assess practical outcomes including operator profit gains, reductions in grid electricity purchases, achievable redirection demand, and associated environmental benefits.

The proposed methods are applied to the Greater Gothenburg region under a 50 % EV adoption scenario. The case study incorporates detailed road networks, public transport timetables, and heterogeneous charger specifications. A synthetic population of 557 220 commuter agents produces fine-grained charging profiles, demonstrating the influence of price-responsive and behavior sensitive modeling (Paper II). The optimization then identifies the cost-optimal mix and location of home (7 kW), slow (11 kW), medium (22 kW), and fast (50 kW) chargers co-located with PV and BESS capacity, balancing operator profit with system cost (Paper III). The findings provide a realistic and data-driven basis for evaluating the technical and economic feasibility of RES integrated charging infrastructure in urban contexts.

Through these work, this thesis aims to answer the following research questions. This thesis establishes reproducible approaches including agent-based charging demand forecasting and strategic infrastructure planning with system cost and benefit assessment for urban transport electrification.

- **Behavior-aware spatiotemporal charging demand forecasting:** How to incorporate price-responsive and smart charging behavior into agent-based modeling with daily travel pattern simulations to produce high resolution spatiotemporal EV charging demand forecasts?

- **Joint charging and energy infrastructure optimization:** How can multi-class charger siting, PV capacity allocation, and BESS scheduling be co-optimized in an optimization to minimize annualised infrastructure and electricity procurement costs?

- **Renewable integration impact:** How much can co-located PV and battery storage reduce peak grid imports and total system cost?

- **User Incentive charging demand management:** To what extent can spatially-targeted user incentives and demand redirection smooth charging demand peak loads and enhance operator net-profit?

- **Case-study validation:** How does the integrated framework perform, both in terms of spatiotemporal charging patterns and optimal infrastructure deployment in a realistic case study of Gothenburg, Sweden?

Disposition of this thesis

This thesis comprises five chapters, followed by the appended research papers (List of Publications). Chapter 2 presents a comprehensive literature review on EV charging demand estimation, PDS interactions, and charging infrastructure planning, and identifies the research gaps addressed in this thesis. Chapter 3 details the integrated methodological framework, including the extended MATSim based Agent-Based Modeling (ABM) for high resolution and behavior sensitive charging demand estimation (Paper II) and the Mixed-Integer Linear Programming (MILP) formulation for strategic deployment of multi-class chargers, PV generation, and BESS with operation optimization and system benefit assessment (Paper III). Chapter 4 reports the application of proposed approaches to a 50 % EV adoption scenario in Gothenburg, describing data preparation, outputs, optimization results, and key insights. Chapter 5 summarizes the main findings, discusses limitations including the aggregate treatment of PDS constraints and exclusion of Vehicle to Grid (V2G) interactions, and outlines directions for future research.

The appended papers provide the full manuscripts and author contribution statements, supporting the summary and analysis presented in the main chapters.

Chapter 2

Literature Review

This chapter reviews key research on transport electrification, drawing on the synthesis presented in Paper I. The review is structured into three thematic areas that directly align with the thesis contributions. Section 2.1 discusses methodological trends and gaps in spatiotemporal EV charging demand estimation. Section 2.3 examines interactions between EV charging and the PDS, including grid impacts and mitigation strategies with emerging smart technologies such as V2G. Section 2.2 surveys charging infrastructure optimization studies, considering both transport system perspectives and integrated approaches that incorporate RES and PDS constraints.

2.1 Charging Demand estimation

Charging demand estimation forecasts the spatiotemporal energy requirements of EVs, providing the basis for charging infrastructure deployment and PDS management. This is distinct from charging activity, which records individual charging events in simulation outputs (Yang et al., 2023; Radermecker and Vanhaverbeke, 2023). Accurate demand estimates are critical for sizing charging infrastructure and for validating model performance (Arias and Bae, 2016). Underutilization of stations, often linked to accessibility, compatibility, or socioeconomic disparities (Yi et al., 2022), can create network imbalances and inequitable service provision, underscoring the need to capture spatiotemporal demand patterns. Supporting even a single EV can raise residential electricity consumption by nearly 50 % (Brouwer et al., 2013), with level 1 chargers typically used overnight at home. By contrast, level 2 and level 3 chargers, prevalent in public, workplace, or commercial settings, impose larger coincident loads and significantly reshape peak demand patterns (Xu et al., 2017; Ermagun and Tian, 2024; Lou et al., 2024). In line with prior reviews (Goh et al., 2022), modeling approaches can also be distinguished by their horizon of application, from short-term forecasts for operational scheduling to long-term projections for strategic planning and policy analysis.

2.1.1 Traditional rule-based and dynamic models

Early static models applied fixed load profiles or static origin destination matrices, treating charging demand as temporally invariant and assuming homogeneous user behavior (Sreekumar and Lekshmi, 2024). While computationally efficient, these methods lack realism in heterogeneous urban contexts and fail to capture variability in demand (Deb et al., 2018b; Hüttel et al., 2021). Rule-based approaches use simple heuristics, such as instructing all vehicles to charge when SoC falls below 20 %, but do not consider stochastic travel patterns, charger availability, or user preferences (Çelik and Ok, 2024; Sanami et al., 2025).

Dynamic models incorporate temporal variation and are typically divided into short-term and long-term horizons. Short-term models forecast from minutes to days, supporting operational planning. Classical methods include regression, clustering, and Markov chains with spatial and temporal covariates such as traffic flow and weather (Meyers and Yang, 2022). Nonlinear approaches, including random forests and gradient boosting, improve accuracy in mixed continuous categorical data settings (Parishwad et al., 2023). Geospatial analytics and GIS methods map temporal usage patterns but often omit capacity constraints or queuing effects (Khalife et al., 2022; Vansola et al., 2023). Probabilistic models address uncertainties in trip chains, travel times, and battery depletion, offering scenario-based risk assessments (Maity and Sarkar, 2023; Das et al., 2022), though they remain limited by reliance on historical data.

Long-term models, intended for strategic infrastructure planning over months or years, apply time series techniques such as ARIMA, transformer-based models, and ensemble approaches to project broader demand trends at station or zone levels (Kim and Kim, 2021; Sike et al., 2023). More recent work employs deep learning architectures, including spatiotemporal graph convolutional networks, Long Short-Term Memory (LSTM) models, and attention-based transformers, which capture complex spatial and temporal dependencies (Wang et al., 2023; Huang et al., 2023). These methods improve spatial and temporal coverage (Yi et al., 2022; Garrison et al., 2023) but face challenges with generalization, vanishing gradients, and data scarcity for emerging behaviors (Shi et al., 2023; Koohfar et al., 2023).

2.1.2 Agent-based modeling frameworks

ABMs represent individual commuters, with explicit daily activity chains, travel choices, and charging behavior, producing high resolution and behavior sensitive spatiotemporal charging demand profiles. Early work by Novosel et al. (2015) coupled MATSim mobility outputs with EnergyPLAN, an advanced energy-systems analysis model (Lund et al., 2004; Lund and Thellufsen, 2022), to translate travel energy into grid impacts and demonstrated the feasibility of linking transport and energy models, but were limited to home to work routines and excluded explicit charger representation, dynamic tariffs and user behavior adaptive charging strategies. However, that implementation was limited to two daily activities (home and work) and excluded explicit charger representation, dynamic tariffs, and varied charging strategies. Zhuge et al. (2021) extended this by modeling both link and node-based charging facilities in MATSim, showing how spatial layouts influence station choice, but still assumed that agents charge at the nearest available facility regardless of SoC, price incentives, or accessibility.

Subsequent studies have progressively expanded ABM capabilities towards . Yi et al. (2023) applied MATSim at the city scale to estimate public charging demand and optimize station siting using a capacitated maximal-coverage approach, validated against high resolution synthetic and observed data, but without accounting for home charging or ToU pricing, both of which strongly influence demand distribution. On interurban corridors, Wu et al. (2023) modeled SoC and proximity based station selection for long distance trips, though the highway focus limited its applicability to urban multimodal settings. In city contexts, Adenaw and Lienkamp (2021) developed the UrbanEV co-evolutionary extension for MATSim, embedding multi-criteria convenience and preference factors into charging decisions. Their work relied on simplified behavioral calibration and excluded explicit responses to price variability. Fadranski et al. (2023) combined MATSim travel patterns with spatial optimization via a genetic algorithm to balance capital costs and user detours in Berlin, but the model lacked temporal demand variation and smart charging incentives. Large-scale applications by Muratori et al. (2021) and Menter et al. (2023) demonstrated the potential of ABM for integrated energy mobility planning, while Lin et al. (2024) surveyed driver-behavior influences on charging distribution. Both emphasized the need for dynamic tariff integration and richer behavioral heterogeneity. Behavioral archetypes such as "plan ahead" and "event triggered" charging strategies are documented, yet they are rarely operationalized within large-scale ABMs. Wongsunopparat and Cherian (2023) examined consumer adoption factors without translating findings into charging-behavior simulations, and Hartvigsson et al. (2022) mapped geographic patterns of power-system violations without modeling diverse charging strategies.

In summary, ABMs address many limitations of static and dynamic forecasting by capturing individual routines, stochastic travel patterns, and facility interactions. Yet no existing framework integrates complete daily activity chains, heterogeneous charger classes, dynamic ToU tariffs, and probabilistic smart charging at the urban scale. Paper II addresses this by embedding a stochastic smart charging module within the MATSim scoring function, enabling agents to reschedule charging during plugged-in windows based on cost, convenience, and range anxiety. To address these gaps, Paper II embeds a stochastic smart charging module within the MATSim scoring function, enabling agents to optimize charging decisions based on cost, convenience, and range anxiety, thereby generating high resolution, behavior sensitive charging demand forecasts.

2.2 Optimal deployment of Charging Infrastructure

Planning EV charging infrastructure involves two key decisions, spatial siting (where to locate charging stations) and charger sizing (how many units and what power classes). These decisions influence user accessibility, travel time, and system cost, and also interact with PDS limits such as voltage stability and thermal capacity. Although most studies approach planning from either a transport system or PDS perspective, integrating RES is essential for the sustainable development of coupled transport and power systems, as illustrated in Figure 2.1. The literature can be grouped into transport system oriented optimization, which treats demand and grid conditions as exogenous, and integrated planning, which jointly considers chargers, RES, and PDS constraints.

Figure 2.1: RES integrated transport electrification

2.2.1 Standalone optimization of charging infrastructure

Early work formulated siting as a network location problem, such as maximal coverage, p-median, or flow refuelling variants, to maximize coverage or minimize detours, typically assuming demand fixed in space and time. Data-driven siting using large-scale mobility traces has shown how heuristic and exact formulations can reduce excess travel while limiting the number of stations (Vazifeh et al., 2019). Decomposition methods such as Benders and column generation allow tractable solutions under probabilistic reachability and range uncertainty, but generally omit renewables and tariff dynamics (Lee and Han, 2017). The Restriction Fragment Length Polymorphism (RFLP) generalisation with Benders decomposition has improved scalability for intercity corridors (Arslan and Karaşan, 2016). Recent reviews summarise siting and sizing formulations, identifying trade-offs between coverage, cost, and equity, and note that many models remain static with respect to temporal demand variation and grid constraints (Ahmad et al., 2022; Çelik and Ok, 2024).

Time and price signals or ToU are more often considered in operational rather than siting objectives. Empirical analysis of non-residential charging in Northern California shows that controlled charging within parking windows combined with ToU tariffs can cut peak contributions by up to 40 % and shift demand to off-peak hours, demonstrating the value of tariff-aware operation even when locations are fixed (Kara et al., 2015). In fleet and logistics contexts, joint routing and charging formulations increasingly account for incentive mechanisms and spatiotemporal prices, using bi-level or decomposition approaches; these can lower operator costs but generally assume a predetermined network (Yao et al., 2023).

Public transport applications introduce additional constraints from timetables and layover durations. Integrated planning models co-optimize charger placement with charging and scheduling decisions to minimize annual costs or energy penalties. Recent work allows flexible public transit timetable adjustments and both depot and on-route charging options (Duan et al., 2023; Gairola and Nezamuddin, 2023). Extensions have added energy storage at depots and explicitly incorporated ToU tariffs and capacity charges into the operating objective (Zhong et al., 2024a). Despite these advances, most transport-focused studies continue to treat charging demand as exogenous and to simplify interactions with PDS and RES.

2.2.2 Integrated charging infrastructure planning

A second stream of research couples siting and sizing decisions with the energy supply side. Reviews of energy planning emphasize the need to impose distribution network limits, including voltage stability and thermal loading, and to co-optimize supply options such as grid connection, on-site PV, and BESS to mitigate local peaks and reduce connection costs (Ahmad et al., 2022). At the station level, recent models determine PV and BESS capacities together with operational schedules to shave peaks and lower energy costs, often using mixed-integer or conic optimization with explicit solar generation profiles (Dong et al., 2024; Huang et al., 2024; Dai et al., 2019). In extreme fast-charging and highway contexts, joint optimization of PV, BESS, and grid supply has been shown to improve economics under both demand and irradiance uncertainty (Liu et al., 2021). At the city scale, energy mobility studies highlight the role of BESS in matching variable RES output to EV demand and in alleviating feeder congestion (Fachrizal et al., 2024).

Demand-side coordination is more often treated as an operational problem after siting decisions have been made. Stochastic and model-predictive control schemes for stations participate in demand response programmes, achieving peak reduction and cost savings through price-based or incentive-based load shifting. However, such approaches typically optimize a single site or operate on a fixed network rather than co-designing locations and capacities (Zanvettor et al., 2024; Casini et al., 2021). Incentive-aware formulations in mobility services confirm that targeted flexibility payments can redirect charging demand in both space and time, but these are rarely embedded within city-wide siting models that also account for RES, BESS, and PDS constraints (Yao et al., 2023). The literature demonstrates three main streams. Mature transport-side siting and sizing models optimized for coverage, cost, and service objectives (Vazifeh et al., 2019; Lee and Han, 2017; Arslan and Karaşan, 2016), station and grid-side models that co-optimize PV-BESS capacity and operation under tariff variation and solar intermittency (Dong et al., 2024; Liu et al., 2021; Šolić et al., 2023), and the operational demand management through demand response and incentives for local peak mitigation (Zanvettor et al., 2024).

Despite progress in each area, there remains a clear gap in urban-scale optimization that *simultaneously* (a) sites and sizes multi-class chargers, (b) sizes and schedules co-located PV and BESS, (c) respects land-use and PDS constraints, (d) uses realistic, behavior-driven demand profiles, and (e) incorporates price and incentive-based redirection. This gap motivates the optimization framework presented in Paper III and discussed later in this thesis.

2.3 Interactions with Power Grid

The accelerated adoption of EVs requires a detailed assessment of PDS impacts and the effectiveness of mitigation measures. This section reviews how charging demand influences grid performance and summarizes strategies such as demand response, RES BESS integration, smart grid controls, and V2G that can improve voltage stability, relieve thermal constraints, and enhance reliability. Demand response refers to actions within the PDS that reduce demand during peak periods and increase it during off-peak periods, with users acting as active participants in system balancing. Electrification of passenger transport adds new stresses to the PDS, including transformer and feeder loading, voltage stability issues, and potential reliability risks. Here, feeders are the set of distribution branches that extend from the source to load areas, delivering power to end users. Understanding these interactions is essential for designing operational strategies and infrastructure investments that maintain power quality and resilience.

2.3.1 Grid impact of charging

Uncoordinated charging can overload transformers and feeders, increase system losses, and cause voltage deviations. These risks are most pronounced during evening peaks and in dense urban feeders. Studies using standard IEEE radial test systems (Deb et al., 2018a; Shukla et al., 2019) and both real and synthetic feeder models (Banol Arias et al., 2018; Jones et al., 2021) consistently report thermal and voltage violations under high EV penetration. Large-scale geographic analyses further show that violation risks vary spatially and seasonally; urban areas and price-optimized charging can worsen low-voltage problems, whereas rural feeders are generally less constrained (Hartvigsson et al., 2022).

Mitigation strategies can be grouped into siting and operational measures. On the siting side, placing public chargers to balance feeder loading can improve voltage profiles and reduce overload events (Nugraha et al., 2023). On the operational side, coordinated or price-responsive scheduling reduces simultaneous charging events and flattens peaks (Bouhouras et al., 2022). Power quality concerns, such as voltage unbalance and harmonics at the end of long feeders, motivate the use of local filtering, inverter-based mitigation, managed charging, and V2G support (Kumar et al., 2021). Long-term analyses indicate that hosting capacity depends on tariff structures and the proliferation of fast chargers and BESS, although integrated assessments of these factors are still limited (Polat et al., 2023; Khan et al., 2019). Overall grid reliability is ultimately linked to targeted reinforcements such as transformer upgrades or network sectionalising, as well as advanced operational tools including voltage optimization and state estimation, particularly under increasing RES and EV penetration (Bibak and Tekiner-Mogulkoc, 2021; Ghania et al., 2022).

2.3.2 Grid mitigations via smart technologies

Smart charging strategies can be implemented in centralized form, controlled by an aggregator or distribution system operator, or in decentralized form, where users respond to broadcast price signals (Xu et al., 2018). Empirical and simulation studies report substantial benefits. In non-residential contexts, price-aligned control can reduce coincident peaks and lower monthly electricity bills (Kara et al., 2015). City-specific assessments reveal heterogeneous gains across private, commercial, and fleet segments (Jian et al., 2018). Comparative analyses indicate that loss-oriented scheduling can reduce network losses, while cost-oriented scheduling lowers electricity procurement costs (Khalid et al., 2024). Incorporating marginal carbon intensity into charging schedules can further reduce emissions relative to uncontrolled charging (Li et al., 2023; Zhong et al., 2024c).

V2G extends these capabilities by enabling bidirectional power flow, allowing EVs to contribute to peak shaving, frequency regulation, and local voltage support (Hu et al., 2016). Recent planning models co-optimize V2G-enabled charger siting with operational strategies under both public and private charging modes, explicitly representing user PDS interactions (Niu et al., 2024). At the microgrid scale, studies examine the economics of V2G for ancillary services when combined with on-site RES and storage (Pilotti et al., 2023). Cost benefit analyses for managed charging show that tariff-aligned control can deliver significant peak reduction and bill savings in non-residential settings, even without full bidirectional capability (Kara et al., 2015). However, few works jointly optimize long-term V2G scheduling with spatial infrastructure planning under distribution constraints (Chauhan and Jain, 2024). Only a small number of studies embed smart charging or V2G control within large-scale demand simulations, which limits the co-design of infrastructure and operational strategies. Many existing analyses rely on coarse hourly time steps, missing sub-hourly peaks that can stress network assets. There is a clear need for frameworks that integrate transport ABMs with feeder-resolved PDS simulations to evaluate infrastructure investments alongside operational controls. This motivates future research that links behavior sensitive demand from our agent-based framework with detailed distribution grid models to co-design tariffs, incentives, and operational strategies.

Synthesis: Drawing together from this literature review, several critical gaps emerge that shape both the contributions of this thesis and priorities for future research.

- *Charging demand estimation:* Many forecasting approaches treat demand as exogenous, static, or only weakly sensitive to user behavior, which limits their ability to reproduce the spatial and temporal patterns of charging in cities. Recent ABM studies with MATSim demonstrate that microscopic activity chains can produce accurate charging demand estimates and inform location optimization. However, typical implementations still simplify the interaction between home and public charging and under-represent price responsiveness.
- *Integrated charging with RES and smart systems:* Transport-focused siting and sizing models often achieve good spatial coverage but omit co-sizing of RES and BESS or realistic tariff signals. Conversely, many station-level energy models co-optimize PV, BESS, and operations but assume fixed networks and static demand. There is a need to co-design charger locations, capacities, and on-site energy resources under time-varying prices and solar availability. Smart charging and incentive-based redirection of EV users have shown promise for peak reduction but remain underused in holistic planning. Future work should incorporate driver acceptance functions for travel distance and time-cost trade-offs directly into network-wide siting and operational decisions.
- *Integrated behavioral-grid modeling:* Evidence from distribution network studies shows that uncoordinated charging can cause transformer and feeder overloads and voltage deviations. Coordinated or tariff-aligned control mitigates these impacts, yet most urban siting models still abstract away feeder constraints and reliability indicators. Future extensions should incorporate detailed grid power flow modeling to improve system resilience and support decarbonisation objectives.

These gaps motivate the integrated pipeline developed in this thesis. User behavior sensitive, agent-based charging demand estimation (Paper II), and city-scale co-optimization of multi-class chargers with co-located PV and BESS under time-varying tariffs (Paper III). The framework provides a basis for extending future work to embed feeder-level PDS constraints and services. Promising directions beyond the present scope include coupling the optimization with feeder-resolved hosting-capacity limits and voltage objectives; extending to bidirectional services (V2G) with joint siting and scheduling under user acceptance and market participation; and developing hybrid modeling approaches that combine activity-based simulation with data-driven forecasting to capture nonlinear behavioral adaptation over time. Addressing these priorities would advance the next generation of EV electrification studies, linking detailed behavioral demand models with robust infrastructure and energy system optimization to achieve sustainable and cost-effective transport electrification.

Chapter 3

Methodology

Urban transport electrification requires charging and energy infrastructure that is both sufficient to meet demand and strategically designed to minimize cost, grid stress, and environmental impact. Determining where and how much infrastructure to deploy depends critically on accurate forecasts of when and where charging demand will occur (i.e., spatiotemporal charging demand). Without a realistic demand model, investments risk being either undersized, leading to congestion and reliability issues, or oversized, resulting in underutilised assets and unnecessary capital costs.

This thesis develops methodologies for future charging demand estimation and strategic charging infrastructure planning for satisfying spatiotemporal charging demand. The first work extends the MATSim framework with integrated charging behavior modeling and a stochastic and adaptive smart charging module (Paper II). Agents optimize charging timing and location decisions in response to their SoC, charging costs, walking distance, and schedule constraints. This produces behaviorally realistic and price-responsive charging profiles that reflect both planned and spontaneous charging decisions. The second work establishes a mixed-integer linear program (Paper III) to co-optimize charger siting, renewable integration, and BESS operation, with the option to introduce location-specific user incentives that redirect demand toward underutilised infrastructure. This two-stage pipeline bridges the critical gaps identified in the literature review.

The following sections of this chapter describe these two components in detail. Section 3.1 presents the agent-based charging demand model embedded in MATSim, including its data requirements, decision rules, and behavioral parameters. Section 3.2 outlines the strategic optimization model for EV charging infrastructure, PV, and BESS deployment, and explains how the outputs of the first stage feed into the second.

3.1 Agent-based charging demand model considering charging behavior

Estimating realistic spatiotemporal patterns of EV charging demand requires a modeling framework that captures individual travel behavior, system-level transport equilibrium, and the diversity of charging strategies. ABMs are well suited to this task because they simulate each traveller's complete daily activity chain, covering home, work, shopping, and leisure. It also embeds trip generation, mode and route choice, and charging decisions within a unified and probabilistic structure. In contrast to static or rule-based estimators, ABMs can model heterogeneous charging behaviors (immediate event-triggered charging versus delayed plan-ahead strategies), capture the interaction between home, workplace, and public facilities, and account for responses to time-varying tariffs. By combining road network properties, traffic conditions, socio-demographic profiles, and empirical charging behavior, the model produces charging demand profiles that evolve in response to changes in infrastructure and pricing. This addresses a key limitation in much of the literature (Chapter 2), the absence of scalable and behaviorally detailed approaches that generate spatiotemporal charging demand endogenously. The complete nomenclature for the following method is listed in Appendix A.1.

3.1.1 Integrated charging demand estimation

To capture the evolution of charging demand under realistic user decisions and tariff structures, we extend the MATSim co-evolutionary replanning process with an EV-oriented module based on the EV-Contrib architecture (ETH Zürich et al., 2016). Each synthetic agent is assigned an activity plan with explicit timing and mode choice, as well as a vehicle profile specifying battery capacity, energy consumption rate, charger plug compatibility, and access type. As agents move through the road network, their SoC is continuously updated. When the SoC drops below a critical level, or when a planned charging opportunity aligns with cost or convenience preferences, a charging event is dynamically scheduled at a compatible facility. Charger attributes include location, plug type, access classification (home, work, public), outlet count, power level, and pricing scheme, with home chargers following hourly ToU tariffs and workplace or public chargers following fixed rates.

The decision logic is embedded within MATSim's iterative scoring and replanning loop (Figure 3.1). The plan utility combines conventional MATSim activity and travel components with EV-specific terms for charging cost, range anxiety, walking disutility, and state-of-charge penalties (Arabani et al., 2024). This enables agents to weigh travel time, monetary cost, and comfort when selecting charging locations and start times. A stochastic BestScore replanning strategy, augmented with the extended utility, iteratively improves each agent's plan until the system converges to an equilibrium in both mobility and charging behavior. Two behavioral archetypes are implemented to reflect heterogeneity in charging decisions. In the *event-triggered* strategy, agents initiate charging

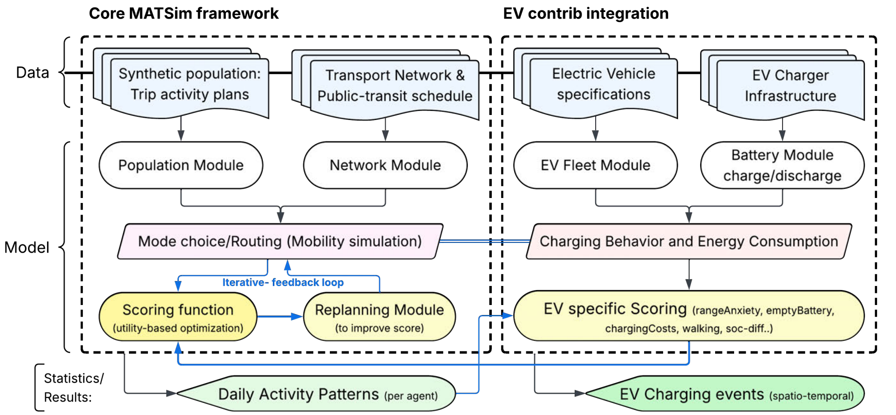

Figure 3.1: Integrated MATSim workflow for EV charging demand estimation

as soon as SoC falls below a defined threshold, regardless of activity duration. In the *plan-ahead* strategy, agents with longer parking durations defer the start of charging to align with lower ToU prices, provided that sufficient SoC is maintained. Start times are chosen through a utility-maximising search within the available parking window. If the required charging time exceeds the idle time, the strategy defaults to immediate charging. The proportions of agents following each strategy are set using two configurable parameters: the *awareness factor*, representing the share of agents who respond to tariff signals, and the *coincidence factor*, representing the likelihood of ignoring price in favour of convenience. These parameters capture heterogeneity in price sensitivity and concurrent charger usage.

The modeling integrates multiple spatial and operational datasets. The road network is derived from processed OpenStreetMap data, with attributes for mode eligibility, capacity, functional class, and free-flow speed. Charger locations are specified in an additional network layer, while agents without assigned home or workplace chargers are probabilistically matched to facilities within a 500 m search radius, assuming 80 % home charger access. Activity plans are generated from empirical distributions of activity types, timings, and spatial locations (Tozluoğlu et al., 2023). Vehicle attributes are defined using MATSim's person and vehicle schema, with energy consumption and battery dynamics determining SoC evolution during trips.

Electricity prices are incorporated through a time-dependent multiplier $M_{\text{temporal}}(t)$ that reflects hourly ToU tariffs. Agents with the "aware" attribute access these prices in real time during simulation, adjusting charging decisions accordingly. Charging demand thus emerges endogenously from the intersection of trip-based energy depletion, charger availability, activity duration, tariff information, and agent-specific decision rules. The simulation is run with a 10 % synthetic population sample, consistent with sampling fidelity studies (Kuehnel et al., 2022), ensuring computational tractability while preserving spatial and temporal resolution. Charger availability is not artificially constrained, allowing charging patterns and load profiles to emerge directly from the interaction of demand, infrastructure, and pricing.

3.1.2 Utility parameters for scoring function

In the MATSim co-evolutionary replanning framework, each agent evaluates its daily activity-travel plan through a pseudo-random utility maximisation process. Alternative plans are scored, compared, and selected probabilistically over successive iterations (Arabani et al., 2024). The base plan utility, S^*_{plan}, aggregates the utilities of activities and the disutilities of travel across all N legs in the plan:

$$S^*_{\text{plan}} = \sum_{q=0}^{N-1} S_{\text{act},q} + \sum_{q=0}^{N-1} S_{\text{trav},q}. \tag{3.1}$$

The activity utility for leg q, $S_{\text{act},q}$, reflects the marginal benefit of remaining at the location for duration $t_{\text{dur},q}$ relative to a reference duration $t_{\text{dur},0}$, and applies penalties for arriving early or late:

$$S_{\text{act},q} = \beta_{\text{dur}} \ln\left(\frac{t_{\text{dur},q}}{t_{\text{dur},0}}\right) + \beta_{\text{early}}\, t_{\text{early},q} + \beta_{\text{late}}\, t_{\text{late},q}. \tag{3.2}$$

Here, β_{dur} denotes the marginal utility of activity duration, while β_{early} and β_{late} are schedule-deviation penalties.

The travel disutility term, $S_{\text{trav},q}$, incorporates a mode-specific constant, travel time, direct monetary cost, travel distance, and transfer penalties:

$$\begin{aligned} S_{\text{trav},q} = {} & C_{\text{mode}(q)} + \beta_{\text{trav,mode}(q)}\, t_{\text{trav},q} + \beta_m\, \Delta m_q \\ & + \big(\beta_{d,\text{mode}(q)} + \beta_m\, \gamma_{d,\text{mode}(q)}\big) d_{\text{trav},q} + \beta_{\text{transfer}}\, x_{\text{transfer},q}. \end{aligned} \tag{3.3}$$

Table 3.1: Default utility parameters for the Urban EV module

Parameter	Value	Parameter	Value	Parameter	Value
$T_{\text{simulation}}$	170 h	$N_{\text{agentPlans}}$	5	$\beta_{\text{emptyBattery}}$	-30.0
$d_{\text{walk,max}}$	500 m	$\text{thres}_{\text{SoC}}$	20%	$\beta_{\text{rangeAnxiety}}$	-10.0
$p_{\text{replan,nonCrit}}$	0.3	$N_{\text{maxChanges}}$	5	β_{walk}	-1.0
$p_{\text{timeAdjustment}}$	0.1	$t_{\text{flexibility}}$	1200 s	β_{socDiff}	-5.0
$c_{\text{homeCharging}}$	1.5	$c_{\text{publicCharging}}$	5.5	$c_{\text{workCharging}}$	5.0
β_{money}	1.0	$\beta_{\text{temporalCost}}$	1.0	$\beta_{\text{chargerCost}}$	1.0

To model EV-specific charging behavior, S^*_{plan} is extended with additional components representing monetary charging cost, range anxiety, battery depletion, walking distance to chargers, and a penalty for finishing the day with a lower

SoC than at the start:

$$
\begin{aligned}
S_{\text{EV, plan}} = S^*_{\text{plan}} &- \beta_{\text{money}}\, C_{\text{charging}} + \beta_{\text{rangeAnxiety}}\, S_{\text{rangeAnxiety}} \\
&- \beta_{\text{emptyBattery}}\, S_{\text{emptyBattery}} - \beta_{\text{walking}}\, S_{\text{walking}} - \beta_{\text{SoCdiff}}\, S_{\text{SoCdiff}}.
\end{aligned}
\tag{3.4}
$$

The extended terms are defined as follows:

Charging cost utility

$$
C_{\text{charging, a}}(t) = E_{\text{consumed, a}}(t) \cdot C_{\text{charger}} \cdot M_{\text{temporal}}(t) \tag{3.5}
$$

where $E_{\text{consumed, a}}$ is the charged energy for agent a (kWh), C_{charger} is the charger type specific price, and $M_{\text{temporal}}(t)$ is the dynamic ToU multiplier for simulation time t.

Range anxiety penalty

$$
S_{\text{rangeAnxiety, a}} = \begin{cases} \beta_{\text{rangeAnxiety}} \cdot \frac{\text{thres}_{\text{SoC}} - \text{SoC}_a}{\text{thres}_{\text{SoC}}}, & \text{if } \text{SoC}_a \leq \text{thres}_{\text{SoC}} \\ 0, & \text{otherwise} \end{cases} \tag{3.6}
$$

Battery depletion penalty

$$
S_{\text{emptyBattery, a}} = \begin{cases} \beta_{\text{emptyBattery}}, & \text{if } \text{SoC}_a = 0 \\ 0, & \text{otherwise} \end{cases} \tag{3.7}
$$

Walking disutility

$$
S_{\text{walking,a}} = \beta_{\text{walk}} \cdot \left(1 - \exp\left(-\lambda \cdot \frac{d_{\text{walk,a}}}{d_{\text{walk,max}}}\right)\right) \tag{3.8}
$$

where $d_{\text{walk,a}}$ is the straight-line distance from the charger to the activity location, and λ controls decay rate.

SoC differential penalty

$$
S_{\text{SoCdiff, a}} = \beta_{\text{socDiff}} \cdot \max\big(0, \text{SoC}_{\text{start, a}} - \text{SoC}_{\text{end, a}}\big) \tag{3.9}
$$

Home charging is not directly rewarded in utility terms but typically yields lower disutility because $C_{\text{homeCharging}} < C_{\text{workCharging}}, C_{\text{publicCharging}}$, allowing tariff differentials to shape location choice.

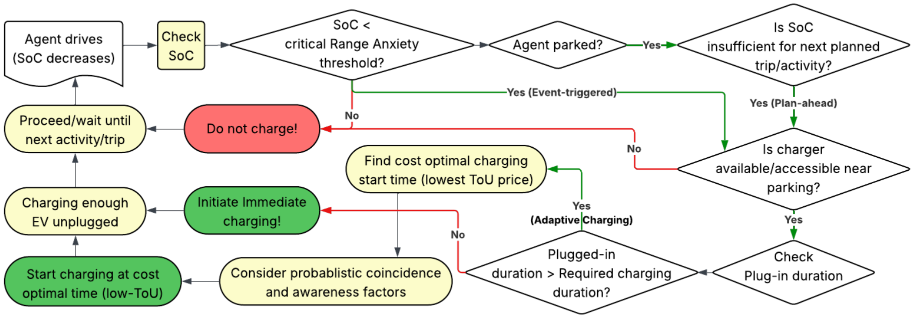

Figure 3.2: Charging decision making logic considering dynamic charging costs

3.1.3 Adaptive smart charging model

The model embeds a novel stochastic smart charging module within MATSim's replanning loop (Figure 3.1), enabling adaptive charging decisions that reflect heterogeneous user behavior (Figure 3.2). Each agent carries a dynamically updated SoC throughout the *mobsim* routine. If the SoC falls below the range-anxiety threshold, an *event-triggered* charging activity is immediately inserted at the nearest accessible and compatible charger, reflecting the high penalties associated with low SoC and battery depletion (Eqs. (3.6)–(3.7)).

If no threshold violation occurs, the model forecasts post-trip SoC. Charging is then considered during the next activity if (a) the projected SoC would breach the threshold and (b) a charger lies within the maximum walking radius (500 m). At this stage, the cost component defined in Eq. (3.5) is applied. Agents with probabilistic price awareness may defer charging within the available dwell window, optimizing for periods of lower ToU tariffs. The actual charging start time is then given by

$$t_{\text{start}}^{\text{opt}} = \arg \min_{t \in [t_{\text{arr}},\, t_{\text{dep}} - T_{\text{charge}}]} \{C_{\text{charging}}(t)\}, \tag{3.10}$$

where $C_{\text{charging}}(t)$ denotes the expected charging cost at time t. Agents lacking price awareness, or with insufficient idle time, default to immediate charging. A coincidence factor introduces additional stochasticity, simulating clustered starts or incidental human delays.

The entire simulation logic is executed within an integrated MATSim framework, and charging is managed intrinsically in this implementation, allowing for the decoupling of plug-in and charging start times, as well as value-of-time and money considerations, vehicle queuing, and unplugging of EVs at activity end. Over successive iterations, the system converges toward a quasi-equilibrium in which charging demand profiles emerge endogenously from the interplay of infrastructure availability, tariff structures, and heterogeneous user responses. During replanning, agents adjust departure times, routes, or charging node choices to improve their overall score. This integrated agent-based model enables the evaluation of demand-shifting effects resulting from pricing information and provides a tractable mechanism for simulating adaptive smart charging behavior under various infrastructural or policy scenarios, which can be scaled up to simulate any region or country.

3.2 Deployment of charging infrastructure with RES and BESS

The second work applies a large-scale mixed-integer optimization model to determine the cost-optimal siting and sizing of public EV chargers, co-located PV capacity, and BESS. This formulation builds on the harmonised spatiotemporal inputs produced in Section 3.3, where agent-based charging events from Section 3.1 are spatially mapped to a common hexagonal grid and temporally aggregated into representative days and intervals. The complete nomenclature is listed in Appendix A.2.

The study area is discretised into hexagonal cells $i \in \mathcal{I}$, each representing a candidate site for public charging infrastructure and on-site energy resources. The planning horizon comprises a reduced set of representative days $m \in \mathcal{M}$ (one per month or season) and half-hourly intervals $t \in \mathcal{H}$, allowing seasonal and diurnal variability to be retained at manageable computational cost. Charging demand from the ABM is aggregated by site, day, and interval, and is separated into home and public classes $b \in \mathcal{B}$. This yields demand tensors $D_{i,m,t,b}$ that form the core of the capacity and energy-balance constraints.

Public charging capacity is modeled through integer decision variables $x_{i,c}$ for charger classes $c \in \mathcal{C}$, subject to site-specific capacity limits. Home chargers C_i^{home} are treated as fixed, cost-free capacity external to the charging point operator (Charging Point Operator (CPO)) decision scope. PV deployment is represented by Ψ_i, the number of installed panel units at site i, each with nominal capacity Ψ^{cap} and bounded by land-availability limits $\bar{\Psi}_i$. Battery deployment is represented by Θ_i, the number of storage units at site i, each with rated energy capacity Θ^{cap}, round-trip charge and discharge efficiencies $\eta^{\mathrm{ch}}, \eta^{\mathrm{dis}}$, and an upper bound $\bar{\Theta}_i$. Grid electricity is procured at time-of-use tariffs $\rho_{m,t}$, while PV output is calculated from Ψ_i and exogenous capacity factors $p^{\mathrm{pv}}_{m,t}$ derived from clear-sky or satellite-based irradiance profiles.

To improve utilization and alleviate localised congestion, the model allows incentive-based spatial redirection of public charging demand. Directed arcs $(i, j) \in \mathcal{D}$ define feasible redirection from an overloaded origin cell i to an underutilised destination j within a maximum network distance. Redirection is modeled only when destination capacity is available and when the energy to be shifted exceeds a minimum threshold. For active arcs $(i, j, m, t) \in \mathcal{A}$, the CPO offers a monetary rebate $T_{i,j}$ proportional to the additional travel time, representing compensation for user inconvenience. Redirected volumes are constrained by the receiving site's available charger capacity and by user acceptance assumptions.

By structuring the model around representative days, respective charging demands, site-specific capacity bounds, and cost parameters, the formulation remains transferable to any urban context. When coupled with local inputs for demand, tariffs, solar capacity factors, and siting constraints, it can produce infrastructure portfolios that reflect local travel behavior, energy pricing, and renewable resource availability.

3.2.1 The MILP objective function

The MILP is formulated to determine the annual net profit of the charging point operator (CPO) over the planning horizon, balancing revenues from energy sales against operating costs, user incentive payments, and the amortised cost of infrastructure investments. Let $N_{\text{days}}(m)$ denote the number of representative days for month m and DAYS the total number of days in the year. The objective function is expressed in Equation (3.11).

$$\begin{aligned} \max \quad & \underbrace{\sum_{m \in \mathcal{M}} N_{\text{days}}(m) \times \Big(\text{Revenue}_m - \text{Cost}_m^{\text{grid}} - \text{Cost}_m^{\text{incentive}} - \text{Cost}_m^{\text{slack}}\Big)}_{\text{Annual operating profit}} \\ & - \underbrace{\text{DAYS} \times \Big(\text{CapEx}^{\text{chargers}} + \text{CapEx}^{\Psi} + \text{CapEx}^{\Theta}\Big)}_{\text{Annualised capital cost}}, \end{aligned} \tag{3.11}$$

The *annual operating profit* term aggregates results over all representative months and consists of four components:

Charging revenue: Total income from charging services is computed by multiplying per-kWh tariffs Price_c by the delivered energy $e_{i,m,t,c,b}$ across all cells, intervals, demand classes, and charger types:

$$\text{Revenue}_m = \sum_{i \in \mathcal{I}} \sum_{t \in \mathcal{H}} \sum_{b \in \mathcal{B}} \sum_{c \in \mathcal{C}} \text{Price}_c \times e_{i,m,t,c,b}. \tag{3.12}$$

This covers both directly served demand and any energy delivered to users redirected from other locations.

Grid electricity cost: Energy purchased from the power grid, whether supplied directly to vehicles or used to charge storage, is priced at the applicable time-of-use tariff $\rho_{m,t}$:

$$\text{Cost}_m^{\text{grid}} = \sum_{i \in \mathcal{I}} \sum_{t \in \mathcal{H}} \sum_{b \in \mathcal{B}} \rho_{m,t} \times \Big(g_{i,m,t,b}^{\text{dir}} + g_{i,m,t}^{\text{batt}}\Big). \tag{3.13}$$

User incentive payments: When public charging demand is redirected from an origin cell i to a destination cell j, the CPO compensates the user based on the travel time difference, represented here as a per-kWh rebate $T_{i,j}$:

$$\text{Cost}_m^{\text{incentive}} = \sum_{(i,j)\in\mathcal{D}} \sum_{t\in\mathcal{H}} T_{i,j} \times n_{i,j,m,t}^{\kappa}. \tag{3.14}$$

The variable $n_{i,j,m,t}^{\kappa}$ denotes the number of redirected charging events in the given arc and time slot.

Slack penalty: A penalty is applied to any portion of demand that cannot be met due to insufficient capacity:

$$\text{Cost}_m^{\text{slack}} = \lambda_{\text{slack}} \sum_{i\in\mathcal{I}} \sum_{t\in\mathcal{H}} \sum_{b\in\mathcal{B}} \epsilon_{i,m,t,b}. \tag{3.15}$$

The coefficient λ_{slack} is set at a sufficiently high value to ensure that unmet demand is minimized in optimal solutions.

The *annualised capital cost* term converts up-front investments into equivalent daily annuities using a present-value factor (PVF_g) for each asset type g (slow, medium, fast chargers, PV panels, and battery units), defined as:

$$\text{PVF}_g(r, n_g) = \frac{1}{365} \frac{r(1+r)^{n_g}}{(1+r)^{n_g} - 1}, \tag{3.16}$$

where r is the real discount rate and n_g the asset lifetime in years. These factors are then applied to compute annualised costs:

$$\text{CapEx}^{\text{chargers}} = \sum_{i\in\mathcal{I}} \sum_{c\in\mathcal{C}} \text{PVF}_c \times \rho^c \times x_{i,c}, \tag{3.17}$$

$$\text{CapEx}^{\Psi} = \sum_{i\in\mathcal{I}} \text{PVF}_{\Psi} \times \rho^{\Psi} \times \Psi_i, \tag{3.18}$$

$$\text{CapEx}^{\Theta} = \sum_{i\in\mathcal{I}} \text{PVF}_{\Theta} \times \rho^{\Theta} \times \Theta_i. \tag{3.19}$$

In combination, Equations (3.11) (3.19) provide a unified framework in which both the operational and investment dimensions are optimized simultaneously. This enables the joint evaluation of charging revenues, energy procurement strategies, incentive-based demand management, and the deployment of PV and BESS assets within a consistent economic objective.

3.2.2 Infrastructure capacity and demand fulfilment constraints

The model limits the number of public chargers that can be installed in each grid cell $i \in \mathcal{I}$ to respect space and land-use constraints:

$$\sum_{c\in\mathcal{C}} x_{i,c} \le \overline{C}_i^{\text{pub}}, \quad \forall i \in \mathcal{I}. \tag{3.20}$$

Here, $x_{i,c}$ is the integer count of chargers of type c, and $\overline{C}_i^{\text{pub}}$ specifies the maximum allowable number of public units in cell i.

At any month m and time interval t, total dispatched charging energy across all demand classes must not exceed the installed technical capacity:

$$\sum_{b \in \mathcal{B}} \sum_{c \in \mathcal{C}} e_{i,m,t,c,b} \ \leq \ \sum_{c \in \mathcal{C}} K_c \, x_{i,c}, \quad \forall \, i, m, t. \tag{3.21}$$

The term $e_{i,m,t,c,b}$ represents energy delivered to class b by chargers of type c at cell i.

Home charging demand benefits first from the capacity of pre-installed chargers $\overline{C}_i^{\text{home}}$, each with power K_{home}. Any remaining load is met by public infrastructure or penalised through slack.

$$\sum_{c \in \mathcal{C}} e_{i,m,t,c,\text{home}} + \epsilon_{i,m,t,\text{home}} = \max\{0, \ D_{i,m,t,\text{home}} - K_{\text{home}} \, \overline{C}_i^{\text{home}}\}. \tag{3.22}$$

Similarly, public charging demand in each cell is balanced by local service and the net effect of redirections:

$$\sum_{c \in \mathcal{C}} e_{i,m,t,c,\text{public}} + \epsilon_{i,m,t,\text{public}} = D_{i,m,t,\text{public}} - \sum_{j:(i,j) \in \mathcal{D}} z_{i,j,m,t} + \sum_{j:(j,i) \in \mathcal{D}} z_{j,i,m,t}. \tag{3.23}$$

Slack variables $\epsilon_{i,m,t,b}$ are penalised in the objective to enforce near-complete demand fulfilment wherever feasible.

3.2.3 Energy balance and renewable-integration constraints

For every cell, representative month, and time interval, total energy supplied from the grid, on-site PV, and BESS discharge must equal the energy delivered to EVs:

$$g_{i,m,t,b}^{\text{dir}} + \text{pv}_{i,m,t,b}^{\text{dir}} + d_{i,m,t,b}^{\text{dis}} = \sum_{c \in \mathcal{C}} e_{i,m,t,c,b}, \quad \forall \, i, m, t, b. \tag{3.24}$$

PV output, whether consumed directly or routed into storage, is limited by the installed panel capacity Ψ_i, per-panel rating Ψ^{cap}, and the time-varying capacity factor $p_{m,t}^{\text{pv}}$:

$$\text{pv}_{i,m,t,b}^{\text{dir}} + p_{i,m,t}^{\text{batt}} \ \leq \ \Psi^{\text{cap}} \, \Psi_i \, p_{m,t}^{\text{pv}}, \quad \forall \, i, m, t. \tag{3.25}$$

3.2.4 Battery scheduling and operational constraints

The BESS state-of-charge SoC $\chi_{i,m,t}$ evolves over time according to the following continuity equation:

$$\chi_{i,m,t} = \begin{cases} \alpha\,\Theta_i\,\mathrm{Cap}^{\Theta}, & t=1,\ m=1, \\ \chi_{i,m-1,|\mathcal{H}|}, & t=1,\ m>1, \\ \chi_{i,m,t-1} + \eta_{\mathrm{ch}}\big(g^{\mathrm{batt}}_{i,m,t} + p^{\mathrm{batt}}_{i,m,t}\big) - \frac{1}{\eta_{\mathrm{dis}}}\sum_{b\in\mathcal{B}} d^{\mathrm{dis}}_{i,m,t,b}, & t>1, \end{cases} \tag{3.26}$$

where α is the initial SoC fraction, η_{ch} and η_{dis} are charging and discharging efficiencies, and Cap^{Θ} is the capacity of a single battery unit.

The SoC is kept within safe operating limits:

$$\beta_{\min}\,\Theta_i\,\mathrm{Cap}^{\Theta} \ \le\ \chi_{i,m,t} \ \le\ \beta_{\max}\,\Theta_i\,\mathrm{Cap}^{\Theta}. \tag{3.27}$$

To prevent simultaneous charging and discharging, a binary mode indicator $\delta_{i,m,t}$ is used:

$$g^{\mathrm{batt}}_{i,m,t} + p^{\mathrm{batt}}_{i,m,t} \ \le\ M\,\delta_{i,m,t}, \quad \sum_{b\in\mathcal{B}} d^{\mathrm{dis}}_{i,m,t,b} \ \le\ M\,(1-\delta_{i,m,t}), \quad \forall\, i,m,t, \tag{3.28}$$

where M is a suitably large constant.

The number of battery units is an integer variable subject to site-specific bounds:

$$0 \ \le\ \Theta_i \ \le\ \overline{\Theta}_i, \quad \Theta_i \in \mathbb{Z}_{\ge 0}. \tag{3.29}$$

3.2.5 Spatial redirection and incentive constraints

Candidate redirection arcs $(i,j) \in \mathcal{D}$ are pre-processed from the road network using a maximum travel distance $d_{\max}$. Only arcs meeting this distance threshold and a minimum demand condition $\kappa_{\min}$ for (i,j,m,t) are retained in set $\mathcal{A}$. The per-kWh rebate for accepting a redirection is calculated as:

$$T_{i,j} = v_{\mathrm{time}}\left(\frac{1}{v_{\mathrm{car}}} + \frac{2}{v_{\mathrm{walk}}}\right) d_{ij}, \tag{3.30}$$

where v_{time} is the user's value of time, and v_{car} and v_{walk} are travel speeds by car and on foot, respectively.

Total incentive expenditure is then:

$$\sum_{(i,j,m,t)\in\mathcal{A}} T_{i,j}\, n^{\kappa}_{i,j,m,t}. \tag{3.31}$$

Each redirected trip consumes on average κ kWh:

$$z_{i,j,m,t} \ \le\ \kappa\, n^{\kappa}_{i,j,m,t}. \tag{3.32}$$

Finally, an arc may only carry redirected flows if activated by binary variable $Y_{i,j,m,t}$, with flows bounded by the capacity at the receiving location:

$$\kappa_{\min} Y_{i,j,m,t} \le z_{i,j,m,t} \le Y_{i,j,m,t} \sum_{c \in \mathcal{C}} K_c \, x_{j,c}, \quad \forall (i,j,m,t) \in \mathcal{A}. \tag{3.33}$$

This MILP framework integrates charger siting and sizing, PV and BESS operation, and spatial demand management under realistic spatial, technical, and behavioral constraints. In its current form, PDS effects are included in aggregate through tariffs and capacity limits; feeder-level impacts such as voltage deviation, thermal constraints, or hosting capacity are not yet explicitly modeled. As discussed in Section 2.3, incorporating such constraints, alongside potential V2G services, remains a key direction for future work.

3.3 Spatiotemporal data integration

The abovementioned approaches require harmonised spatial and temporal datasets that serve both the agent-based charging demand estimation and the strategic infrastructure deployment optimization. These datasets consist of the synthetic populations, the multimodal transport network, the charging infrastructure, and the temporal energy context, are processed to a common spatial and temporal resolution so that the outputs from the ABM can be directly utilised in the MILP framework.

3.3.1 Synthetic population and activity-travel patterns

The ABM is initialised with a synthetic population that captures the heterogeneity of urban travellers (Tozluoğlu et al., 2023). Each agent is assigned a daily activity plan, consisting of ordered sequences of activities such as home, work, shopping, and leisure, with geocoded origins and destinations, start times, and durations drawn from household travel surveys or diary datasets (ETH Zürich et al., 2016). Socio-demographic attributes, including age, employment status, income group, and vehicle ownership, influence travel demand, mode choice, and the likelihood of charger access (Westin et al., 2018). For EV-owning agents, battery capacity, energy consumption rate, and plug compatibility are specified in line with observed fleet compositions. These attributes are encoded using MATSim's XML schema and govern the iterative mobility-charging decision process described in Section 3.1.

3.3.2 Transport network and charging infrastructure

Routing, mode choice, and charger accessibility assessments rely on a multimodal transport network and a detailed charger inventory. The network, derived from cleaned OpenStreetMap data and General Transit Feed Specification (GTFS) feeds, is converted into MATSim-compatible XML with attributes such as link capacity, free-flow speed, mode eligibility, and transit timetables (Calazans Campelo et al., 2017; Fayyaz S. et al., 2017). Charger locations are

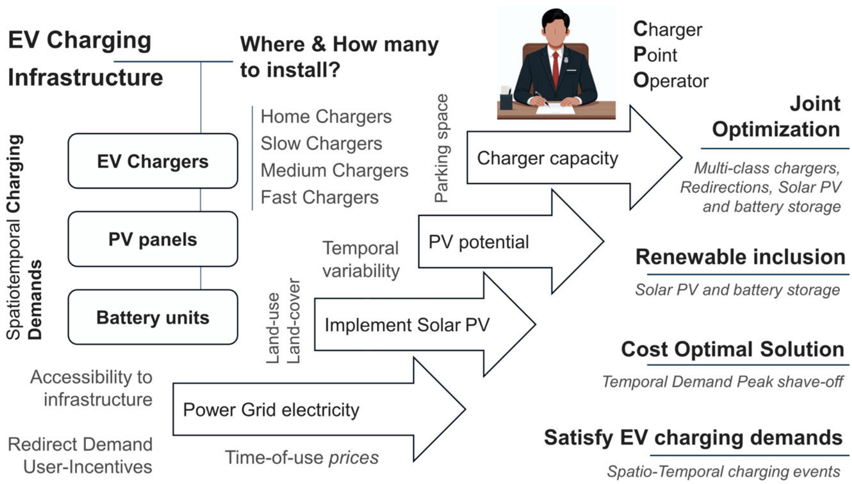

Figure 3.3: Overview of data streams and their role in the optimal charging-infrastructure framework

represented as georeferenced points classified by power class, plug type, and access category (home, workplace, or public) (Erbaş et al., 2018). Land-use layers, building footprints, and parking polygons provide constraints for feasible charger placement and maximum site density (Csiszár et al., 2019; Abdullah et al., 2022). All spatial layers are projected to a common coordinate reference system and overlaid on a uniform grid, which defines the candidate site set $i \in \mathcal{I}$ for the optimization stage (Section 3.2).

3.3.3 Dynamic tariffs and RES generation profiles

Temporal datasets supply the dynamic context for charging decisions in the ABM and operational scheduling in the MILP. Electricity tariffs are sourced from day-ahead market data, adjusted for taxes, network charges, and retail margins, and expressed as hourly or half-hourly price series. In the ABM, these prices enter the decision logic through the time-dependent multiplier $M_{\text{temporal}}(t)$ (Birk Jones et al., 2022; Yang et al., 2024). Renewable generation is represented through monthly-by-hour PV capacity factors, obtained from clear-sky models or satellite-based irradiance datasets, which determine the temporal coincidence between local generation and charging demand (Ameur et al., 2020; Liu and Du, 2023).

3.3.4 Spatial and temporal aggregation

The ABM produces millions of timestamped charging events, each with location, energy charged, and charger type. These events are spatially mapped to their host grid cell and temporally aggregated into representative periods and discrete time intervals (48 half-hour slots), producing a demand tensor $D_{i,m,t,b}$ over sites i, representative periods m, time intervals t, and charger classes b. This aggregation ensures that high resolution charging patterns from the behavioral simulation are directly compatible with the spatial and temporal discretisation used in the MILP constraints as per Equations (3.22) to (3.23).

By aligning all spatial layers, activity-travel attributes, tariff profiles, and renewable output data within a single reference system and discretisation scheme, the integrated pipeline ensures that demand forecasts from the ABM can be seamlessly converted into infrastructure and operational decisions in the optimization model. This harmonisation improves reproducibility, enables consistent sensitivity analysis under alternative infrastructure or tariff scenarios, and makes the approach transferable to other urban contexts without modification to the underlying framework.

3.3.5 Land-use and land-cover constraints

Realistic infrastructure planning must account for spatial limits on the installation of charger and PV infrastructure. These limits are determined by available Land-Use and Land-Cover (LULC) spatial capacities, parking capacities, and consideration for pre-existing chargers. They are implemented in the optimization model as upper bounds on the corresponding decision variables, ensuring that results remain physically and legally feasible for any study region.

Public-charger capacity bounds: For each grid cell $i \in \mathcal{I}$, the maximum number of deployable chargers is linked to the availability of suitable parking spaces. The methodology assumes that each designated public parking can host a charging point, an approach consistent with prior siting studies (Giménez-Gaydou et al., 2016; Bian et al., 2019). Parking inventories can be compiled from LULC analysis or multiple geospatial sources such as municipal parking registers, open data parking lot layers, and volunteered or crowdsourced geographic information, and merged after removing spatial duplicates. The resulting per-cell counts form the charger installation limit (C_i^{pub}), which constrains the public-charger siting decision variables in the optimization framework (see Equation (3.20)).

PV installation potential: PV installation limits are derived from two complementary spatial datasets. First, publicly available parking lot inventories are used to identify areas where full canopy coverage is feasible; here, we assume that 100% of the delineated parking-lot footprint can be considered for PV deployment. Second, high resolution aerial or satellite imagery combined with vector land use and building footprints is classified using supervised LULC mapping techniques applied in solar siting studies (Nanda et al., 2020; Sander et al., 2024). A conservative fraction (10%) of the total available area is assumed suitable for PV deployment, accounting for shading, access, and structural constraints. This area is converted into a maximum number of PV panels per cell ($\overline{\Psi}_i$) which acts as the PV capacity bound in the optimization framework (see Equation (3.25)).

Private-home charger inputs: Existing private home chargers are treated as exogenous charging capacity, available to meet residential demand before any public infrastructure deployment. The potential stock is estimated from residential building footprints classified as eligible single-family dwellings and filtered for minimum floor area. An assumed penetration rate (50%) is applied to represent the share of eligible dwellings equipped with chargers. The resulting fixed counts (C_i^{home}) enter the optimization directly in the residential-demand balance equations (see Equation (3.22)), preventing the model from oversupplying public chargers in areas already well served by private home charging infrastructure.

By incorporating LULC, parking, and building footprint datasets into spatial bounds, this methodology ensures that all charger and PV siting outcomes respect practical feasibility constraints, enabling direct transfer of the framework to different regions without altering the underlying optimization logic. In Chapter 4, we apply the discussed methodology to a real-world case study, examining the resulting infrastructure mix and evaluating the role of renewables and incentive mechanisms in achieving a cost-effective and resilient EV charging ecosystem.

Chapter 4

Analysis, Results and Insights

This chapter summarizes the results of applying the developed methods from Chapter 3 to the Greater Gothenburg region in Sweden. The analysis links the agent-based charging demand estimation with the subsequent infrastructure optimization to interpret the system-level impact insights. We first restate the main case-specific inputs to ensure transparency and traceability of assumptions for Gothenburg, Sweden, and point back to Chapter 3 for data definitions and preprocessing steps. The datasets conform to the spatiotemporal backbone (Section 3.3) introduced earlier, with a hexagonal grid for location analysis and monthly representative days for seasonally resolved operations. We then present the outputs of charging demand estimation, including the EV SoC dynamics, temporal demand profiles, and spatial demand. Next, we report the optimal infrastructure optimization and operational schedules, covering charger deployment, PV and BESS operation, grid purchases under ToU tariffs, and the effects of RES integration and user incentive-based redirection on peak load and system cost. The chapter concludes with key insights and targeted sensitivity analyses for the Gothenburg context.

4.1 Case Study in Gothenburg, Sweden

To demonstrate and validate the proposed methods, we configure a near future scenario with 50% EV penetration for the Greater Gothenburg area in Sweden. The study region demarcation follows Trafikverket's Region A zoning and encompasses Gothenburg Municipality together with the adjoining municipalities of Partille and Mölndal. This area includes a dense urban core with extensive public transport coverage, suburban neighbourhoods, and peri-urban corridors (Figure 4.1). Such heterogeneity in land-use and travel behavior provides a case study for both the charging demand estimation and the subsequent optimization of charging and energy infrastructure.

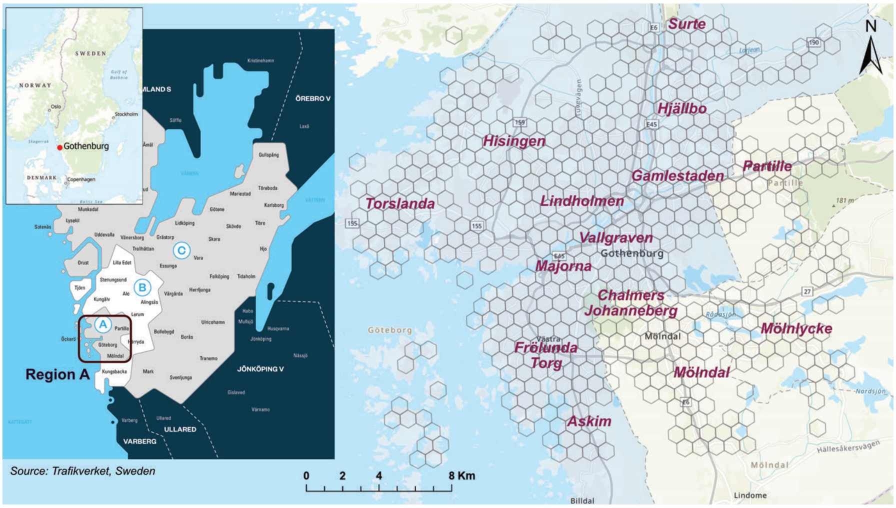

Figure 4.1: Study area (Region A, Trafikverket) within Greater Gothenburg, Sweden.

All case specific datasets are pre-processed to match the uniform spatial grid and temporal resolution as defined in Chapter 3, ensuring consistency across both modeling stages. The spatial discretisation uses a uniform hexagonal grid (Section 3.3), while the temporal resolution adopts monthly representative days, each split into 48 half-hour intervals, to capture diurnal and seasonal variability.

4.1.1 Synthetic population and activity travel data

The synthetic population with activity patterns for the MATSim stage (Section 3.1) comes from the Synthetic Sweden Mobility (SySMo) work (Tozluoğlu et al., 2023), which integrates socio-demographic records from Statistics Sweden, the national travel survey, and land-use based origin–destination matrices from the Sampers model (Parishwad and Jia, 2023). Each synthetic individual is assigned relevant socio-demographic attributes and a complete daily activity chain. Activity chains comprise ordered sequences of activity types (home, work, shopping, leisure) with geocoded coordinates, start and end times, durations, and selected travel modes.

For this case study, the synthetic population dataset contains 557,220 individuals within the study footprint. Of these, 211,880 are designated as car users. A 50% EV penetration rate is assumed among car users, yielding 105,945 EV agents, with the remainder using conventional vehicles, public transport, walking, or cycling. These population and activity travel attributes are encoded in MATSim's XML schema, as described in Section 3.3.1, and form the basis for generating location specific, time dependent charging events.

4.1.2 Electric vehicle fleet specifications

Each EV-owning agent in the synthetic population is assigned a vehicle from a representative set of market-available models in Sweden, spanning multiple size and performance classes (Table 4.1). The selected models (BMW i3, Renault ZOE, Tesla Model Y, Volvo XC40 P8, and VW ID.4) reflect a mix of compact, mid size, and sport utility categories observed in recent registration statistics. For each vehicle type, the simulation uses manufacturer derived specifications for battery capacity, rated energy consumption, and maximum charging C-rate, along with compatibility for home, workplace, and public chargers as defined in Section 3.3.

These technical parameters govern the achievable driving range, charging duration, and infrastructure compatibility in (Section 3.1). The initial SoC for each EV is drawn from a uniform distribution between 60% and 80%, representing typical post-trip battery levels. To capture heterogeneity in user behavior, additional attributes, including range-anxiety thresholds and flexibility in shifting charging within a parked interval, are assigned at the agent level. Range anxiety attribute is included for every EV agent in their trip activity, with a uniform distribution between 15% and 25%, representing typical EV user behavior statistics.

Table 4.1: **EV model attributes and fleet counts**

Vehicle model	Consumption (kWh/100 km)	Battery (kWh)	Max C-rate (C)	Count
BMW i3	21.0	42	2.0	2 205
Renault ZOE	17.2	52	1.5	2 126
Tesla Model Y	18.3	75	2.0	2 064
Volvo XC40 P8	15.6	60	1.5	2 107
VW ID.4	16.3	34	2.0	2 092

4.1.3 Charging infrastructure and accessibility

The charging network in the MATSim scenario comprises three charger types-home units (7 kW), workplace units (11 kW), and public stations (22 kW, ten outlets per site) (Table 4.2). Home and workplace chargers are assumed to be present at 80% of eligible residential and office locations, based at the end of agent work and home designated trips. Charger assignment to agents follows their dwelling or workplace location, with availability constraints as specified in Section 3.3. Public charging stations are positioned to provide coverage in areas of high residential or employment density, along major transport corridors, and near key trip attractors. The base dataset contains 796 public stations, of which 662 register non-zero utilization in the simulated day. For all charger types, accessibility is subject to a maximum walking distance of 500 m between the activity location and the charging point.

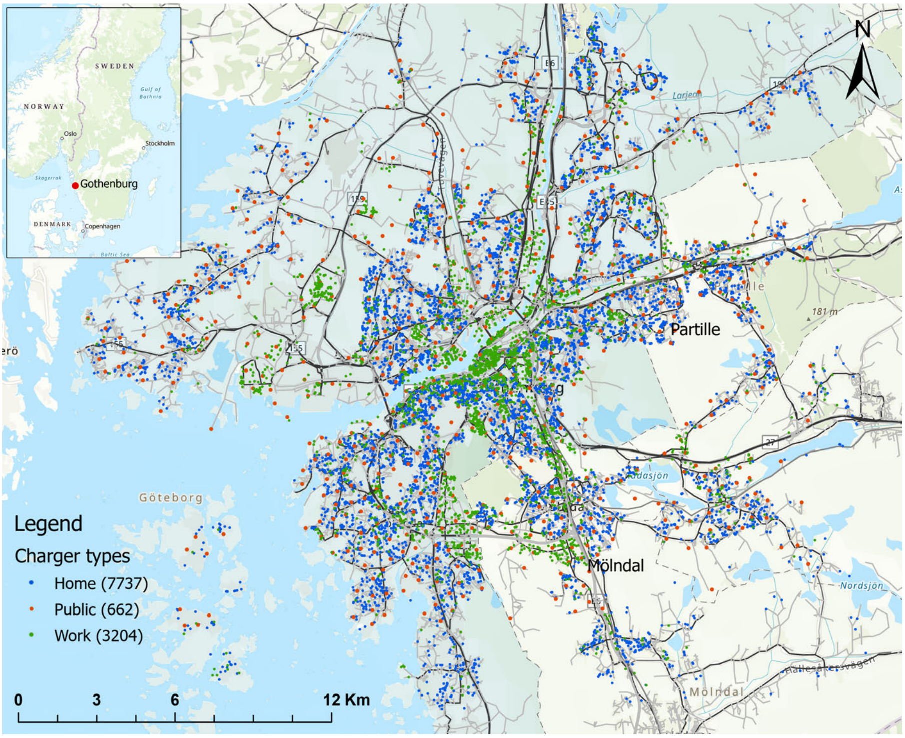

Figure 4.2: Spatial distribution of MATSim simulated chargers in Gothenburg

4.1.4 Transport network and public transit schedule

The multimodal network illustrated in Figure 4.2 is used in the MATSim stage (Section 3.1), which integrates road and public transit datasets to enable realistic route choice, trip chaining, and mode switching. Road geometry and attributes are sourced from Open StreetMap (OSM) and include free-flow speeds, link capacities, and permitted modes. All spatial data layers, including agent origins and destinations, are projected to the `SWEREF 99 TM` coordinate system (EPSG:3006), providing a consistent metric scale for distance and accessibility calculations.

Public transport services are incorporated using GTFS feeds from regional operators, covering bus, tram, ferry, and commuter rail services. The public

Table 4.2: **Charger infrastructure summary**

Charger type	Power	Outlets/station	Total stations	Used stations
Home	7 kW	1	8 475	7 737
Work	11 kW	1	8 475	3 204
Public	22 kW	10	796	662

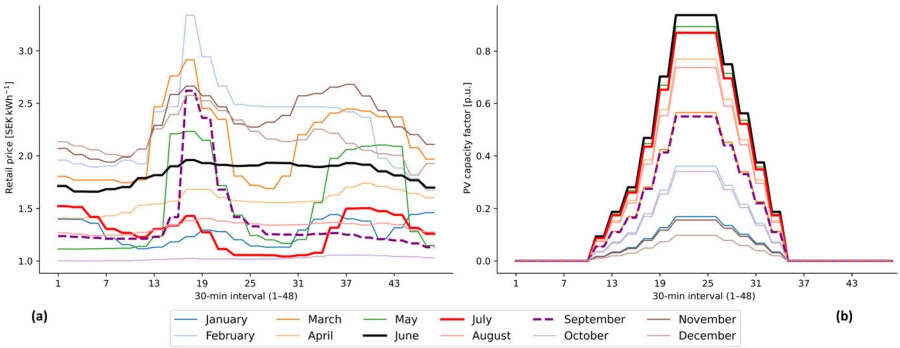

Figure 4.3: Gothenburg temporal datasets, monthly profiles (a) Retail grid electricity pricing; (b) Clear sky PV capacity factors

transit layer includes routes extending slightly beyond the Region A boundary to capture transfers, waiting times, and availability effects that influence mode choice for agents whose trips cross municipal borders. Ferry services on the Göta älv and selected coastal routes are also included to reflect waterborne travel options. The GTFS timetables and stop locations are converted to MATSim schedules with defined stops, lines, and vehicle blocks, enabling time-resolved simulation of multimodal accessibility. Congestion effects on road travel are represented through link-based volume–delay functions calibrated to reflect observed peak-period delays in the Gothenburg region.

4.1.5 Nordpool electricity tariffs and PV generation

Electricity price and PV generation data are required. In the MATSim simulation, ToU home-charging tariffs influence charging start times and location choice for price-responsive agents, while fixed workplace and public charging prices reflect typical local market rates. In the MILP optimization (Section 3.2), the same retail tariffs $\rho_{m,t}$ enter the grid procurement cost term $\mathrm{Cost}_m^{\mathrm{grid}}$, and PV generation limits are enforced through constraints.

Hourly day-ahead spot prices for the Swedish bidding area SE3 are obtained from Nord Pool[1] and converted to retail prices by adding regulated Swedish charges: electricity tax (0.375 SEK/kWh), grid fee (0.45 SEK/kWh), retailer margin (0.02 SEK/kWh), and 25% VAT. This yields seasonal variation, with winter (Dec–Feb) averages around 2.00 SEK/kWh and summer (Jun–Aug) averages near 1.50 SEK/kWh. Intra-day spreads exceed 0.50 SEK/kWh, peaking at 0.70 SEK/kWh on spring mornings. Representative hourly multipliers used in the MATSim charging decision logic are listed in Table 4.3. Nord Pool data show clear seasonal variation, with average summer prices of about 15–20% lower than winter prices. In Gothenburg, winter months (Dec–Feb) average around 2.00 SEK/kWh, while summer months (Jun–Aug) average about

[1] https://www.nordpoolgroup.com/en/market-data12/Dayahead/Area-Prices/SE/Hourly/, accessed July 2024

1.50 SEK/kWh (Figure 4.3a). Within each season, peak-to-off-peak spreads exceed 0.50 SEK/kWh, with the largest spread (0.70 SEK/kWh) seen on spring mornings. While the MATSim considers annual average of the dynamic tariff values (Table 4.3), this seasonal variation in the electric tariff is considered in the optimization framework (Figure 4.3a).

Table 4.3: **Hourly price multipliers for home charging tariffs**

Time window	Multiplier	Charging cost
00:00–06:00	0.70	Low
06:00–08:00	1.60	High
08:00–10:00	1.47	High
10:00–17:00	0.92	Medium
17:00–20:00	1.14	High
20:00–22:00	1.00	Medium
22:00–24:00	0.70	Low

PV generation inputs for the optimization are expressed as monthly-by-hour capacity factors $p^{\mathrm{pv}}_{m,t}$ derived from the JRC PVGIS (v5.3) database (European Commission. Joint Research Centre., 2025). These factors combine clear-sky irradiance models with historical weather data for Gothenburg, capturing both diurnal production profiles and seasonal variation. At this latitude (57.7°N), summer midday clear-sky capacity factors can reach 0.90 p.u. (per unit of installed capacity), while winter midday peaks are close to 0.10 p.u., an order-of-magnitude difference in generation potential. Average summer monthly factors are about 0.20, dropping to approximately 0.01 in mid-winter. The PVGIS factors used here have been validated against measured PV plant data in Sweden, showing mean absolute errors below 10% for monthly yields (Formolli et al., 2023). Figure 4.3(b) shows aggregated seasonal profiles for clarity, but the MILP model uses separate values for each month to represent the full annual cycle.

4.1.6 Charging infrastructure install limits

In the Gothenburg case, spatial limits for charger and PV deployment are derived from high resolution parking and land use datasets for Gothenburg, Partille, and Mölndal. These limits enter the optimization model as the public charger bound (C_i^{pub}), the PV capacity bound ($\overline{\Psi}_i$), and the fixed home charger availability (C_i^{home}).

Public charger capacity: A comprehensive inventory of public parking capacity was compiled by merging multiple geospatial sources: the open-data parking lot layer[2] from Göteborgs Stad, OSM data tagged as `amenity=parking` or `amenity=charging_station`, and parking registers from the neighbouring municipalities of Partille and Mölndal. After removing spatial duplicates, parking locations were aggregated into the common hexagonal grid (Section 3.3)

[2] https://data.goteborg.se/ParkingService/v2.3/help, accessed August 18, 2025

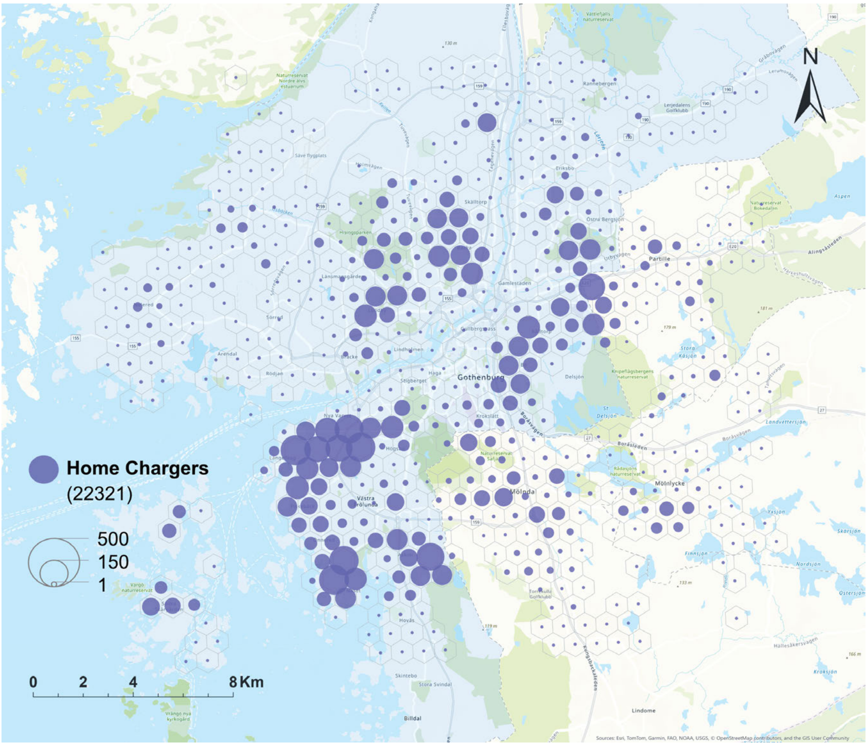

Figure 4.4: Home chargers per hex-grid cell for the Gothenburg region. Counts are based on eligible single-family dwellings with 50% EV penetration.

to compute a per-cell installation capacity. The modeling assumption is that each parking bay can host one charging point, consistent with prior siting studies (Giménez-Gaydou et al., 2016; Bian et al., 2019).

PV installation potential: The PV installation limit in each grid cell is estimated from two spatial sources. First, mapped parking-lot footprints are extracted from OSM and municipal geodata. These areas are assumed to be fully usable for canopy-based PV deployment, consistent with recent urban solar siting practices. Second, adjacent public land and open surfaces are identified through LULC classification and supervised multispectral satellite imagery analysis, following approaches in European PV potential studies (Sander et al., 2024). For these broader classified areas, only a conservative fraction (10%) of the surface is considered suitable for PV deployment, accounting for shading, accessibility, and structural constraints. The combined PV installation potential is 100% of the parking lot footprint plus 10% of the classified public land area is converted into a maximum number of standard 400 W modules per grid cell, which defines the PV installation bound used in the optimization framework.

Fixed home chargers: Private home chargers are treated as fixed capacity within the optimization framework, available to meet residential charging demand before any public deployment. Counts are based on OSM building footprints tagged as `building=villa`, `detached`, or `bungalow`, filtered for a minimum floor area of $25\,\mathrm{m}^2$. Applying the 50% EV penetration assumption to eligible single-family dwellings yields the fixed charger count in each grid cell. Figure 4.4 maps the resulting spatial distribution, showing concentrations in higher-income detached housing areas such as Majorna (up to 1 520 chargers per cell), and sparse availability (< 10 per cell) in less dense northern districts. By integrating these spatial bounds, the optimization respects physical feasibility and observed infrastructure constraints in the study area.

4.1.7 Infrastructure capital costs and lifetimes

The optimization stage uses 2024–2025 capital cost and lifetime parameters for charger types, PV modules, and BESS, drawn from Swedish and European market data. All costs are expressed in SEK (excluding VAT) and annualised using the present value factor (PVF_g) in Equation (3.16), assuming a uniform real discount rate ($r = 6\%$). This amortisation allows fair comparison of assets with different lifetimes. Public charging tariffs are set in SEK/kWh based on prevailing Gothenburg market rates, with higher values for faster charger types. PV and BESS assets have no retail tariff; their benefit in the optimization is through reduced grid purchases and associated cost savings. Private home chargers are assumed to be user-funded and are excluded from the capital cost and revenue model of the CPO. Table 4.4 summarizes the specifications, unit CapEx, assumed technical lifetime, and applicable tariffs for each infrastructure category. Charger costs reflect installed turnkey prices, PV module costs are per 400 W panel, and BESS costs are per 10 kWh cell.

Table 4.4: CapEx, lifetimes, and tariffs for infrastructure assets (Sweden)

Infrastructure asset	**Specification**	**CapEx**	**Life (yr)**	**Tariff**
"home" charger	7 kW AC	*	10	0.00
Public "slow" charger	11 kW AC	16 000	10	5.50
Public "medium" charger	22 kW AC	22 000	10	6.00
Public "fast" charger	50 kW DC	240 000	10	6.50
Solar PV panel (400 W)	0.4 kW	5 200	25	–
Battery cell (10 kWh)	10 kWh	45 000	15	–

4.2 Charging Demand Results and Insights

The integrated MATSim–EV framework produces high resolution spatiotemporal charging profiles from agents' SoC-aware routing and utility-based charging choices. All simulations converged within 60 co-evolution iterations, at which point agent plan utilities stabilised and a dynamic transport equilibrium was reached, consistent with iterative learning processes in MATSim-type models (Adenaw and Lienkamp, 2021). We first examine individual SoC trajectories, sampled at 15-minute intervals, before moving to aggregate and comparatively

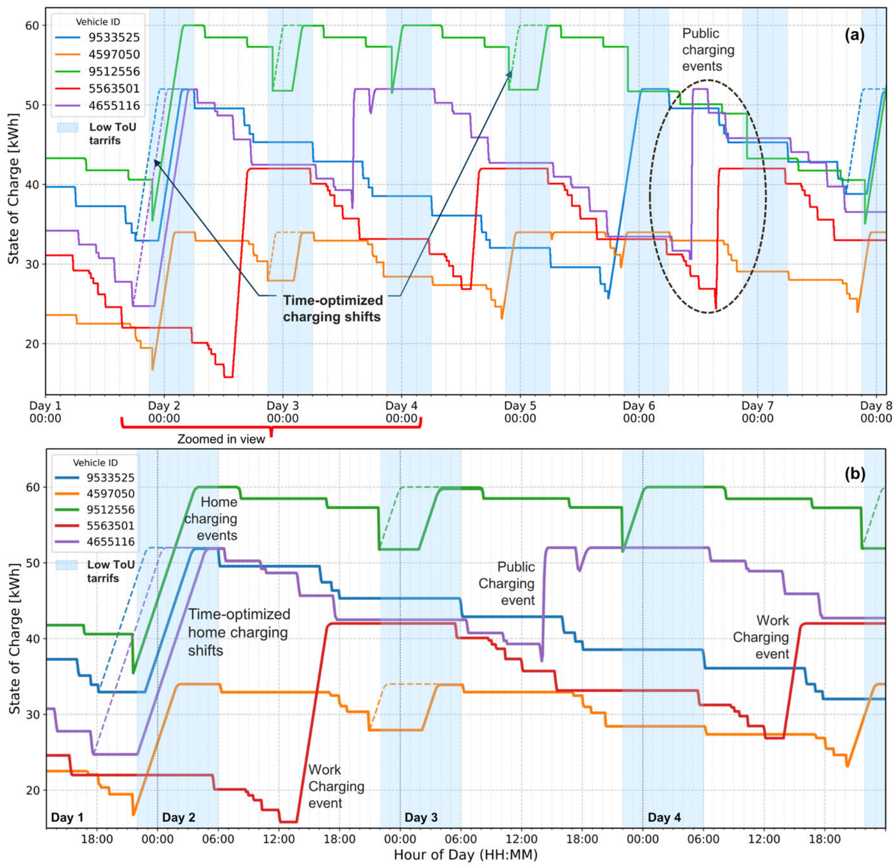

Figure 4.5: (a) SoC trajectories for five EV agents over the simulated week; (b) Zoomed view of SoC profiles.

assess temporal demand patterns under three behavioral-pricing scenarios, and spatial utilization outcomes across the considered Gothenburg region in Sweden (Figure 4.1).

4.2.1 Simulated State-of-Charge dynamics

Figure 4.5 shows one-week SoC profiles for five randomly selected EV agents. The linear charge ramps identify charger type by slope: public chargers (22 kW) exhibit the steepest gradients, workplace chargers (11 kW) are intermediate, and home chargers (7 kW) have the shallowest rise. Effective slopes fall slightly below nameplate values due to vehicle–charger efficiency and taper effects, as represented in the vehicle module (Sevdari et al., 2023). Agents start with an initial SoC between 60 % and 80 %, drawn from a uniform distribution. Across the week, daily depletion is generally 5–15 kWh, consistent with the vehicle-specific consumption rates (15.6–21 kWh/100 km) and observed trip lengths. Off-peak ToU windows (22:00–06:00) are highlighted by shaded bands. In several cases, notably Days 1–3 and Day 4 in the zoomed panel, home-charging events are shifted into these low tariff hours. This shift is visible as delayed start times following evening arrivals, with the dot–dash overlays indicating the adjusted charging periods. The zoomed view (Figure 4.5b) illustrates heterogeneity in charging strategies. Vehicle 9512556 performs a single overnight home session (gain of about 25 kWh over ∼6 h), whereas others fragment charging into multiple shorter sessions aligned with daily activities. Vehicle 4655116 alternates between public and workplace charging, while Vehicle 5563501 relies on intermittent public charging when its SoC nears a driver-specific lower bound, visible on Days 3 and 4. Work charging events are also evident, such as the mid-morning sessions for Vehicle ID 4597050.

Overall, these patterns show that home access enables more consistent overnight charging, while a lack of access to a home charger drives reliance on public infrastructure and greater variation in charging timing. The combination of ToU price sensitivity, range-anxiety thresholds, and charger accessibility results in diverse but realistic SoC trajectories, avoiding critically low levels while exploiting low tariff windows. These microscale behaviors form the basis for the aggregated demand and spatial profiles analysed in the following subsections.

4.2.2 Charging demand profiles: Scenario comparison

The individual SoC trajectories for all EV agents were aggregated to hourly charging loads under three behavioral pricing scenarios (Figure 4.6). Results are scaled from the 10% synthetic population simulation to the full regional fleet at 50% EV penetration. This sampling approach is standard in large-scale MATSim studies and has been shown to preserve temporal patterns when properly scaled.

Scenario 1: Non-cost-aware immediate charging. In the absence of charging costs, agents select charging locations and times solely for convenience (Figure 4.6a). Workplace charging dominates the 06:00–09:00 window, peaking at 32,012 kWh at 07:00 and totalling 275,320 kWh over the day. Home charging forms a broad evening peak at 17:00 (34,576 kWh) and totals 397,074 kWh. Public charging is more evenly distributed, with a mid-morning maximum of 23,614 kWh and a daily total of 304,938 kWh. The temporal shape shows pronounced workplace-arrival peaks and modest overnight home charging, reflecting convenience driven charging behavior (Yi et al., 2023).

Scenario 2: Charger-cost-aware immediate charging. Introducing tariffs (fixed 5.0 SEK/kWh at work and public sites; time-of-use at home) rebalances charging toward the cheaper residential option (Figure 4.6b). Home charging increases by +36.2% from Scenario 1, reaching 540,678 kWh daily, with a higher evening peak at 18:00 of 50,306 kWh (+45.5% vs. Scenario 1).

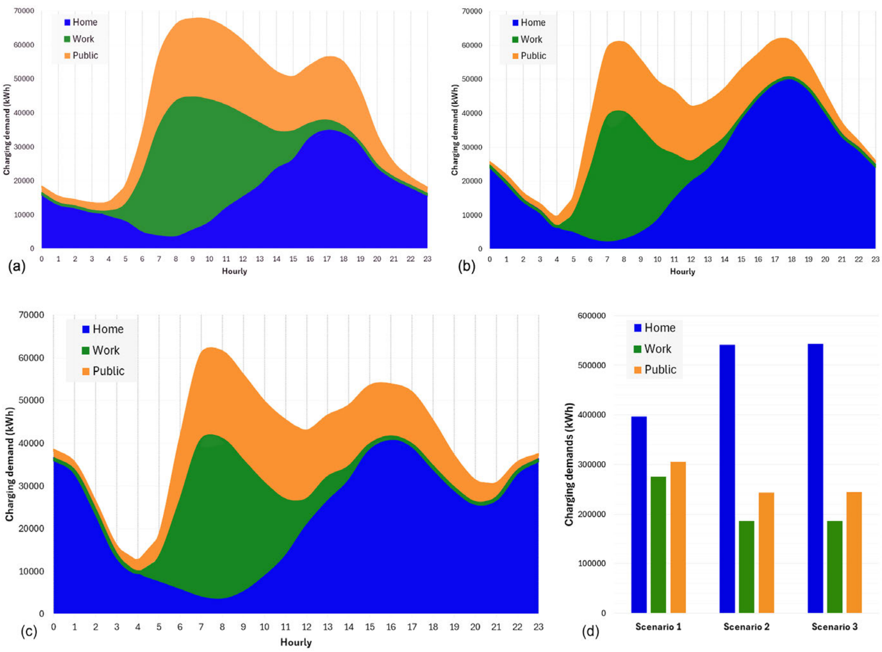

Figure 4.6: Hourly aggregate charging demand by charger type: (a) Scenario 1 (Non-cost-aware immediate charging), (b) Scenario 2 (Charger-cost-aware immediate charging), (c) Scenario 3 (Adaptive cost-aware smart charging), (d) Daily totals by scenario.

Public charging falls by 20.3% to 242,900 kWh, while workplace charging drops by 32.3% to 186,352 kWh. The total daily energy falls slightly to 969,930 kWh (−0.8% vs. Scenario 1), indicating that pricing shifts load location and timing without materially changing total consumption (Khan et al., 2024).

Scenario 3: Adaptive cost-aware smart charging. Allowing 70% of agents to optimize charging start times within plug-in windows (with a 30% stochastic coincidence factor) mitigates the evening home peak (Figure 4.6c). Home charging rises marginally to 542,678 kWh (+0.37% vs. Scenario 2). The 17:00 peak is reduced to 38,996 kWh, a −22.5% drop from Scenario 2 and −11.1% relative to Scenario 1. Off-peak (22:00–06:00) home charging increases by +12,981 kWh (+56.2% vs. Scenario 2), reaching 36,055 kWh at 23:00. Workplace and public charging remain unchanged in daily totals from Scenario 2, at 186,352 kWh and 243,900 kWh, respectively. Total daily energy is 972,930 kWh, only +0.3% from Scenario 2. This probabilistic deferral is consistent with field studies showing that managed charging and ToU incentives shift load to low-price windows without creating rebound spikes at period boundaries (Göberndorfer et al., 2024).

Figure 4.6(d) shows that while total daily energy varies due to stochasticity by less than 1% across scenarios, temporal profiles change substantially. Scenario 2 shifts charging from public/workplace to home in response to cost differences, amplifying evening residential peaks. Scenario 3 achieves the strongest peak reduction, shifting a significant share of residential load into off-peak windows while preserving daytime accessibility to workplace and public charging. These smoothed demand profiles feed directly into the optimization in Chapter 3, where infrastructure portfolios can be tailored to exploit off-peak home charging, manage workplace peaks, and right-size public capacity.

4.2.3 Spatial patterns of charging demand and utilization

Figure 4.7 maps hexagon-level daily charging metrics across Region A (see Figure 4.1 for boundaries).

Figure (a) shows total daily energy delivered per cell. Peripheral suburbs such as Askim, Torslanda, and Partille register under 145 kWh/day, reflecting low charging demand. In contrast, the historic city centre (Inom Vallgraven) and dense mixed-use districts exceed 11,000 kWh/day, with the busiest cells surpassing 20,000 kWh/day. This central–peripheral gradient mirrors the concentration of trip destinations, mixed land uses, and higher EV ownership in the core compared to dispersed residential patterns at the fringe.

Figure (b) reports mean session duration as a proxy for utilization intensity. The shortest averages (< 81 min) occur in outer cells where charging is often opportunistic. Central clusters such as Lindholmen Science Park and Gamlestaden sustain much longer durations, frequently above 520 min and in some cases reaching 645–930 min. These extended times are consistent with all-day parking at home or workplace AC chargers, indicating locations suited to slower charging technologies, whereas short-stay zones could justify higher-power installations.

Figure (c) shows the mean walking distance from the activity location to a used charger. High-density neighbourhoods with on-plot or curbside access average 0–20 m. Peripheral and low-density cells can exceed 300 m, with some island and rural fringe locations (e.g., Öckerö archipelago) reaching 945–1,560 m. As accessibility studies suggest, walking tolerance often drops beyond 300–400 m for routine activities (Daniels and Mulley, 2013), these longer distances signal underserved areas. Strategic infill within 200–300 m of residential clusters could improve user uptake and equity.

Figures (d)–(f) disaggregate demand by charging context. Home charging (Figure d) is concentrated in residential belts, peaking at 4,706–8,350 kWh/day in areas such as Majorna and Frölunda Torg. Workplace charging (Figure e) aligns with employment corridors and campuses, reaching 5,443–14,460 kWh/day in Lindholmen and Chalmers. Public charging (Figure f) clusters at retail and transport hubs (Nordstan, Heden, Frölunda Torg) with 1,047–5,450 kWh/day. These complementary spatial roles match empirical findings that location type is a primary determinant of charging time and place (Kazemtarghi et al., 2024; Potoglou et al., 2023).

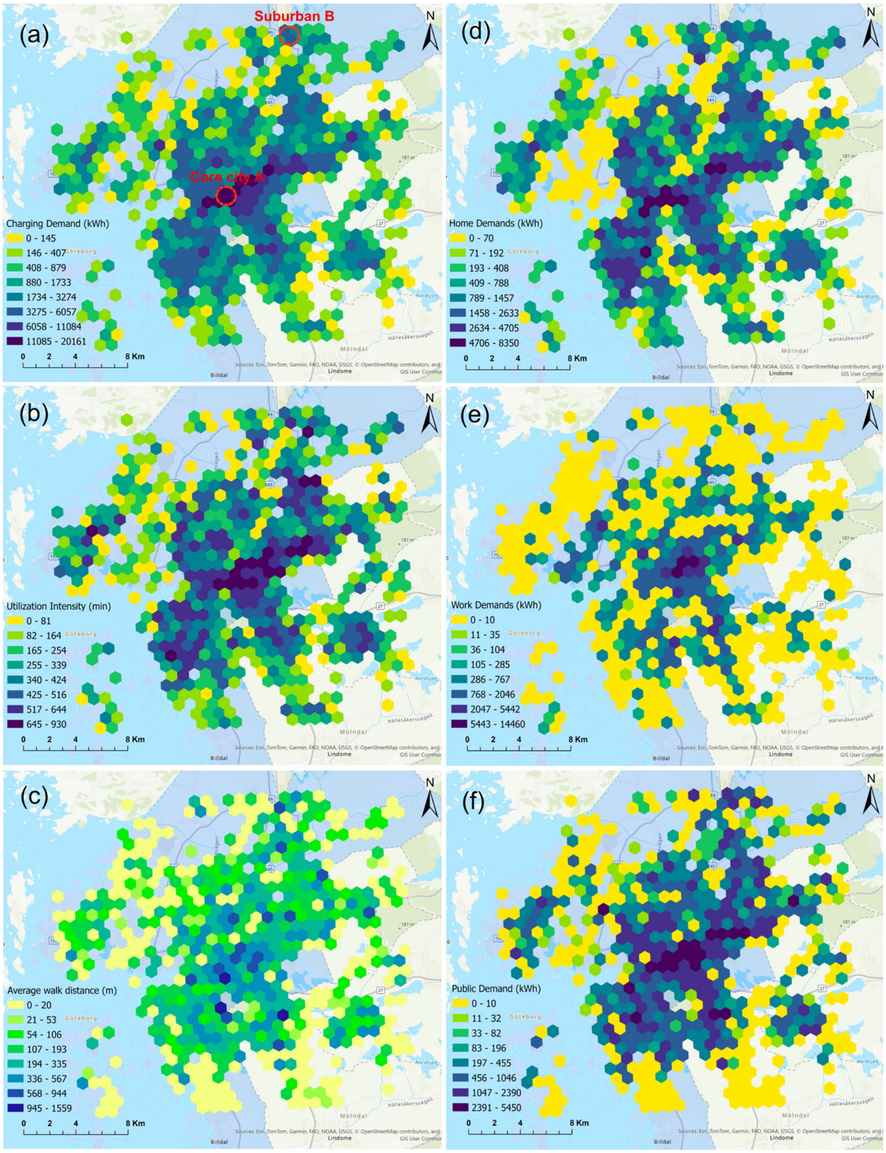

Figure 4.7: Hex-cell aggregates across Region A: (a) total daily charging demand, (b) mean session duration, (c) mean walking distance, and Charging Demands for (d) home, (e) work, (f) public events.

The co-occurrence of high demand and long dwell times in the core suggests deploying additional 50 kW DC fast chargers alongside dynamic load management to reduce queuing during extended AC sessions. At the same time, low-utilization cells with high average walking distances point to opportunities for distributed neighbourhood-scale chargers to balance spatial access and

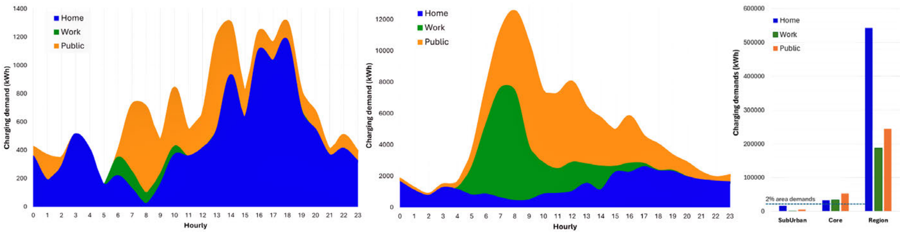

Figure 4.8: Hourly charging demand by location type: (a) Surte (suburban), (b) Central Gothenburg (urban core), and (c) daily totals by type.

reduce user inconvenience.

4.2.4 Local charging demand patterns

To illustrate how local land use and infrastructure access shape temporal charging behavior, two contrasting hexagons from Figure 4.7(a) are examined: a suburban cell in Surte (Ale municipality) and an urban-core cell in Inom Vallgraven (central Gothenburg). Their hourly charging demand profiles are shown in Figure 4.8(a,b), with Figure (c) comparing daily energy totals by location type.

Surte (suburban): Daily demand is modest and spread throughout the day (Figure 4.8a). Home charging dominates, peaking at 1,104 kWh at 16:00, consistent with plan-ahead evening sessions to exploit lower ToU rates. Workplace charging is negligible, with a maximum of 132.5 kWh at 06:00, while public charging reaches 605 kWh at 08:00. Over 24 hours, the cell delivers 16,500 kWh at home, 504.5 kWh at work, and 4,655 kWh at public chargers , about 2.2% of the region's total daily demand (21,660 kWh vs. 972,930 kWh). The strong residential share and weak daytime work/public use reflect low job density and sparse destination charging typical of suburban areas.

Inom Vallgraven (urban core): Demand profiles here are highly concentrated around commute and mid-morning activity peaks (Figure 4.8b). Workplace charging surges to 7,034 kWh between 07:00–08:00, public charging peaks at 6,534 kWh at 09:00, and home charging reaches 2,548 kWh at 17:00. Daily totals are 32,256 kWh (home), 33,854 kWh (work), and 52,102 kWh (public), accounting for over 12% of regional demand within less than 3% of the study area. This concentration aligns with evidence that dense mixed-use cores, abundant charger supply, and high trip density drive spatial–temporal coincidence of demand.

In Surte, the prevalence of evening home charging and minimal midday workplace/public use suggests value in deploying additional workplace AC chargers or small public stations to spread load into daytime hours, improving flexibility and reducing residential clustering after 17:00. In Inom Vallgraven, pronounced morning workplace peaks and substantial public demand indicate the need for high-capacity DC fast chargers and dynamic load management at key nodes to mitigate queuing and local network stress. The agent-based simulation thus identifies where and when charging is likely to occur under current access, ToU tariffs, and user preferences. However, it does not address the cost-optimal mix or placement of infrastructure. In the following section, we apply the MILP optimization framework, which takes the high resolution MATSim demand as input and co-optimizes the siting and sizing of multi-class public chargers, co-located PV and BESS, and tariff-aware operations, with optional spatial redirection incentives. This closes the loop from behavior-driven demand modeling to strategic, economically grounded infrastructure planning.

4.3 Infrastructure optimization results and insights

This section presents the outcomes of applying the optimization model (Section 3.2) to the Gothenburg case study region in Sweden (Figure 4.1). The optimization takes as input the high resolution and behaviorally derived charging demand described in Chapter 4.2.

As detailed in Section 3.3, the agent-based modeling represents approximately 557 220 synthetic agents in the study area, of which about 106 000 are EV users under a 50% penetration scenario. These charging events are aggregated to the spatial and temporal discretisation used in the optimization, at 48 half-hourly intervals for each representative day, mapped across 564 hexagonal grid cells covering Region A. The aggregated demand profiles preserve the results from the final scenario (Figure 4.6(c)). To capture seasonality without prohibitive computational cost, the optimization uses one representative day per month, each resolved at the same 30-minute interval as the input demand data, and scales results to an annual horizon. Sensitivity checks confirm that this representative-day approach reproduces annual profit and deployment estimates within a narrow margin of a full-year run, while reducing solution times by roughly an order of magnitude.

Using these spatio–temporally aggregated charging demands as the fixed demand inputs ($D_{i,m,t,b}$) in the MILP framework, the following analysis evaluates four alternative infrastructure strategies. Each scenario modifies the set of available planning options, such as user redirection, BESS, and co-located PV, to quantify their incremental impacts on network design, operational scheduling, energy procurement, and profitability.

4.3.1 Scenario comparisons: marginal impacts

We assess four scenarios to isolate the incremental effect of different planning features and understand how spatial redirection, battery storage, and co-located PV affect the profitability and operation of EV charging network. All scenarios use the same MILP formulation and constraints discussed in Section 3.2 and the same behavior driven demand inputs. Only the available planning options

Table 4.5: Summary of infrastructure, annual energy flows, costs, and net profit

	Baseline	**Scenario 1**	**Scenario 2**	**Scenario 3**
Infrastructure deployed				
Home chargers (7 kW)	22 321	22 321	22 321	22 321
Slow chargers (11 kW)	287	279	283	284
Medium chargers (22 kW)	7 205	7 229	7 225	7 204
Fast chargers (50 kW)	22	6	6	6
Charger capacity (kWh)	162 767	162 407	162 393	161 912
PV panels	-	-	-	88 886
Battery units (10 kWh)	-	-	70	732
Annual energy (GWh)				
Grid purchase	227.398	227.398	227.398	191.853
Grid→chargers	227.398	227.398	227.129	191.311
Grid→batteriess	-	-	0.00027	0.542
PV produced	-	-	-	35.545
PV→chargers	-	-	-	32.350
PV→batteries	-	-	-	3.195
Demand redirected	-	0.108	0.108	0.929
*Annual costs & profit**				
Local revenue	1478.088	1478.088	1478.088	1478.088
Net Redirection revenue	-	0.596	0.596	5.108
Grid electricity OpEx	392.073	392.073	391.765	332.497
Redirection OpEx	-	0.212	0.212	1.621
Charger CapEx	17.141	16.708	16.703	16.657
PV + battery CapEx	-	-	0.288	34.303
Net profit	1068.873	1069.094	1069.119	1093.009

**All costs are reported in million Swedish krona (SEK) units.*

differ, as the optimal solutions summarised in Table 4.5, and visualised in Figure 4.9, highlight how each feature adds value when integrated into the optimal deployment strategy.

Baseline (chargers Only):

In the absence of PV, BESS, or user redirection, the optimization deploys 287 slow, 7 205 medium, and 22 fast public chargers, totalling 162,767 kWh of rated capacity. All charging demand is supplied by the grid, requiring 227.4 GWh/year. Annual operating costs are dominated by grid electricity purchases (SEK 392 million), with charger capital expenditure at SEK 17.14 million. User charging payments yield revenues of SEK 1.478 billion, resulting in a net profit of SEK 1.069 billion. This serves as the benchmark for subsequent scenario comparisons.

Scenario 1 (Charger + user redirection)

Allowing user redirection of sessions within 1.5 km, supported by targeted incentives, diverts approximately 0.11 GWh/year (≈0.05% of total demand)

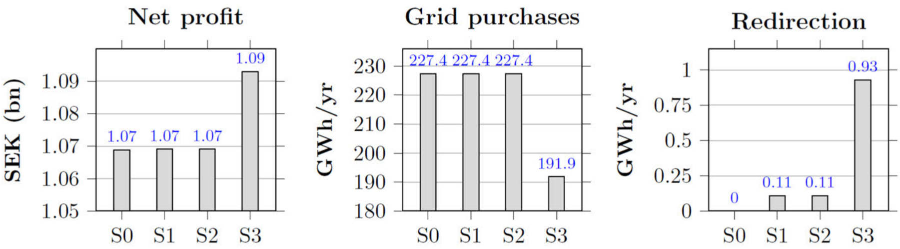

Figure 4.9: Comparative assessment across scenarios.

from congested to underutilised cells. This modest peak shaving reduces fast-charger deployment from 22 to 6 units (–73%) and slightly lowers slow-charger counts, cutting charger CapEx by about SEK 0.43 million/year. Incentive payments remain low (SEK 0.21 million/year), while avoided congestion generates additional revenue of roughly SEK 0.60 million/year. The net profit increases to SEK 1.0691 billion, a marginal gain of 0.02% over the baseline. These small improvements reflect both the limited fraction of demand that is economically viable to redirect and the short walking-distance threshold imposed.

Scenario 2 (Chargers + BESS without PV)

Adding 70 battery units (10 kWh each) of BESS enables tariff arbitrage. Charging during low-cost off-peak hours (269 MWh/year) and discharging at high-cost periods. Charger deployment remains almost unchanged from Scenario 1, so Capital Expenditure (CapEx) differences for chargers are negligible. The additional BESS CapEx of SEK 0.29 million/year yields only a SEK 0.024 million/year profit increase (+0.002% over Scenario 1). Without PV, the BESS simply shifts the timing of grid electricity use rather than substituting a higher cost supply with low-cost renewable energy. This underlines that, in high-penetration AC networks with modest intraday tariff spreads, BESS alone delivers limited financial return unless paired with low-cost generation.

Scenario 3 (Chargers + PV + BESS + user redirection)

Integrating 88,886 PV panels with BESS and redirection changes the economics substantially. The PV array produces 35.55 GWh/year, of which 91% (32.35 GWh) is used directly for charging and 9% (3.20 GWh) is stored in BESS for later use. Annual grid purchases drop by 15.6% to 191.85 GWh/year, cutting electricity expenditure by about SEK 60 million/year. Surplus PV availability makes detours to solar-rich sites more attractive, increasing redirected demand to 0.93 GWh/year, over 8.5 times Scenario 1 levels. While PV and BESS raise infrastructure CapEx to SEK 34.3 million/year, operational savings more than offset this, lifting net profit to SEK 1.093 billion. This represents a 2.24% increase over baseline and the highest performance among all scenarios.

Across the four scenarios, user redirection alone delivers only marginal profit gains, mainly through reducing fast-charger requirements in high demand nodes.

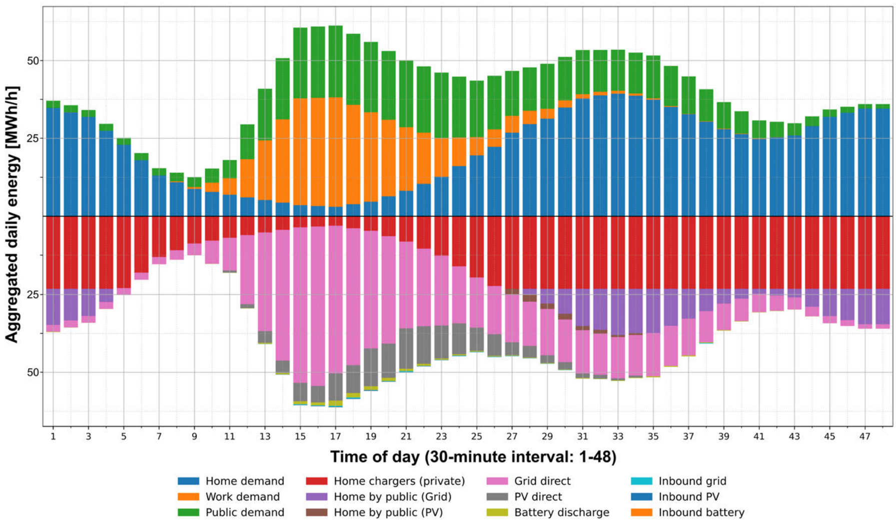

Figure 4.10: Scenario 3: half-hourly charging demand (positive) and supply (negative) on a representative March day in Gothenburg.

BESS without renewables offers negligible additional value in the Gothenburg context, as intraday tariff differentials are modest. The inclusion of PV fundamentally alters the outcome, lowering dependence on grid electricity, enabling greater use of demand redirection, and significantly improving profitability. These results confirm that the most effective strategy combines renewable generation, BESS, and targeted demand management, aligning operational cost savings with infrastructure right-sizing and improved utilization.

4.3.2 Daily demand–supply balance

Figure 4.10 presents the half-hourly charging demand and corresponding supply sources for Scenario 3 on a representative March day in Gothenburg. The positive y-axis aggregates demand from home, workplace, and public charging, while the negative y-axis disaggregates the energy supply by origin, for grid electricity, direct PV generation, and BESS discharge. Privately owned home chargers meet approximately 77% of residential charging needs, concentrated in off-peak night hours and the midday trough between commuting peaks. The remaining 23% of home demand is served by local public chargers, mainly in cells without high home-charger penetration. Midday coincides with the strongest renewable contribution. Direct PV output, supplemented by PV-charged BESS discharge, supplies up to one-quarter of the total charging load. This period overlaps both the highest solar irradiance and elevated ToU grid tariffs, allowing renewables to displace the most expensive grid energy and reduce operator costs.

The BESS operates as a tariff alignment buffer, charging during low-price

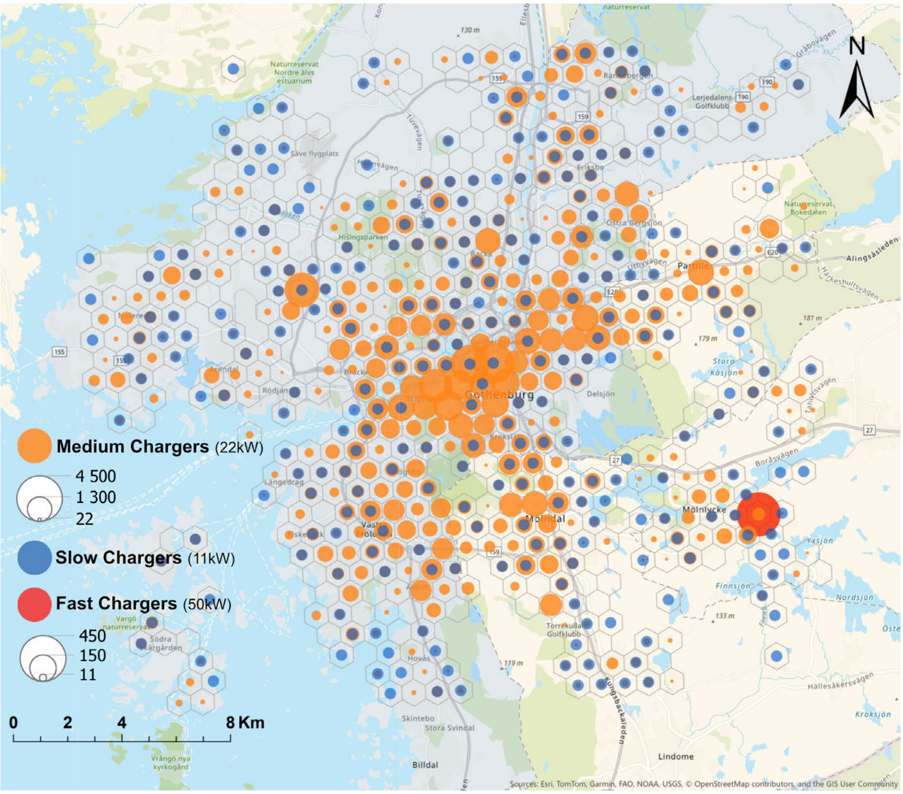

Figure 4.11: Local Capacity (kWh) of Public Chargers per hex-grid cell

intervals (both overnight from the grid and midday from surplus PV) and discharging in the late afternoon and early evening when demand and prices peak. This temporal shifting flattens the net grid draw and reduces the need for high-cost peak procurement. Redirected charging demand, actively steered toward sites with available PV and charged BESS, contributes an additional 5–10% of supply during the busiest afternoon intervals. This dual effect of relieving congestion in peak-demand cells and increasing renewable utilization in surplus cells enhances both service reliability and asset productivity.

The combined operation of PV, BESS, and targeted user redirection substantially reshapes the daily demand–supply profile. Grid reliance drops sharply in the costliest hours, while the renewable share rises in periods of high demand. These patterns reflect the optimization model to co-optimize supply side generation, BESS dispatch, and spatial demand management, yielding both operational and economic benefits in line with observed outcomes from managed charging and co-located PV–BESS deployments (Hull et al., 2024).

4.3.3 Charger deployment patterns

The optimized public charger network is visualized by charger type across the 564 hexagonal cells of Gothenburg Region A (Figures 4.12(a), 4.12(b)). Slow (11 kW) and fast (50 kW) charger counts are shown in Figure 4.12(b), medium (22 kW) charger counts in Figure 4.12(b), and the combined local charging capacity in Figure 4.11.

Medium-speed chargers comprise over 95 % of the public chargers and concentrate along primary commuting corridors and high-activity districts, striking a balance between installation cost and throughput requirements (Figure 4.12(b)). Only six fast chargers are deployed, strategically located at major arterial nodes and park-and-ride facilities to provide rapid top-ups without excessive investment in expensive DC infrastructure (Figure 4.12(a)). The 284 slow chargers fill service gaps in densely populated suburbs, where overnight or long-duration parking makes lower-speed charging sufficient.

Figure 4.11 illustrates the spatial intensity of total public charging capacity (kWh) per cell, confirming that land-use heterogeneity and local demand peaks drive charger type allocation. High-capacity clusters appear in central urban cores and transit hubs, while suburban and fringe areas rely on slower bays. These deployment patterns validate our model ability to align charger typology with spatial variations in EV traffic, residential density, and activity centers, ensuring both coverage and cost-effectiveness.

4.3.4 RES and BESS infrastructure

Co-locating solar PV and BESS with public chargers delivers the largest profitability gains by displacing expensive grid imports and enabling both temporal and spatial load shifting. Figure 4.13 (June representative day) overlays the optimal PV panel installations, BESS allocations, and the peak redirection flows that were determined by the MILP. PV panels cluster in cells that combine high charging demand, available rooftop or parking-lot area, and minimal green-space restrictions. These installations produce up to 35.5 GWh/year, of which roughly 32.4 GWh feeds chargers directly and 3.2 GWh charges the BESS (Table 4.5). High midday irradiance in these cells allows for maximal solar capture precisely when workplace and public demand peaks occur.

BESS deployment (732 $\times$ 10 kWh units) closely follows the PV sites and major commuter corridors (Figure 4.13). The BESS smooths two tariff driven peaks (06:00-09:00 and 16:00-19:00) of a day by charging from surplus PV between 10:00 and 15:00, and from low tariff grid during overnight hours. During high-tariff intervals, batteries discharge up to 1.2 kWh per cell, offsetting grid purchases and shaving peaks.

Figure 4.14 presents the January representative-day SoC trajectories for all BESS units (grey) and their mean SoC (red dashed). Starting at 20%, the BESS charges steadily to 75-80% by late afternoon, then discharges through

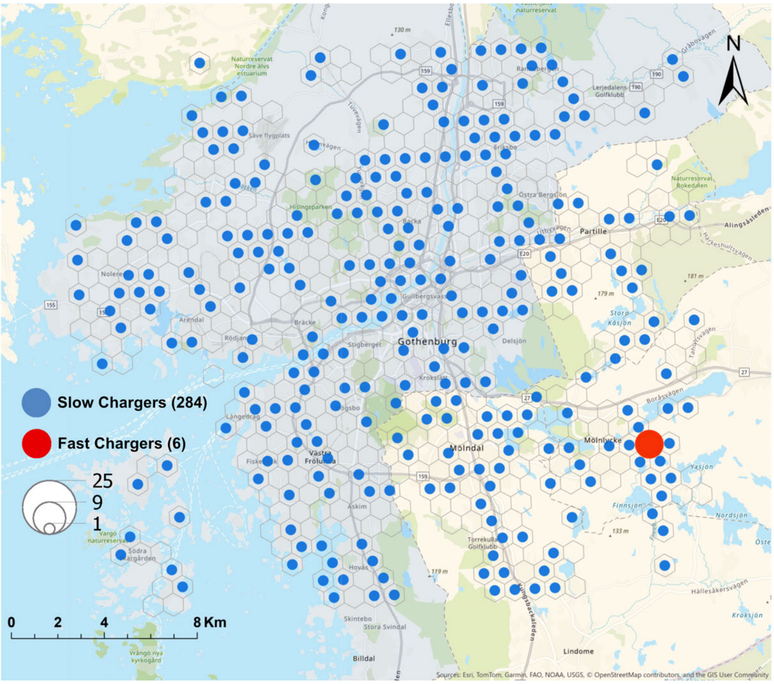

(a) Slow and Fast public charger counts per hex-grid cell for study region

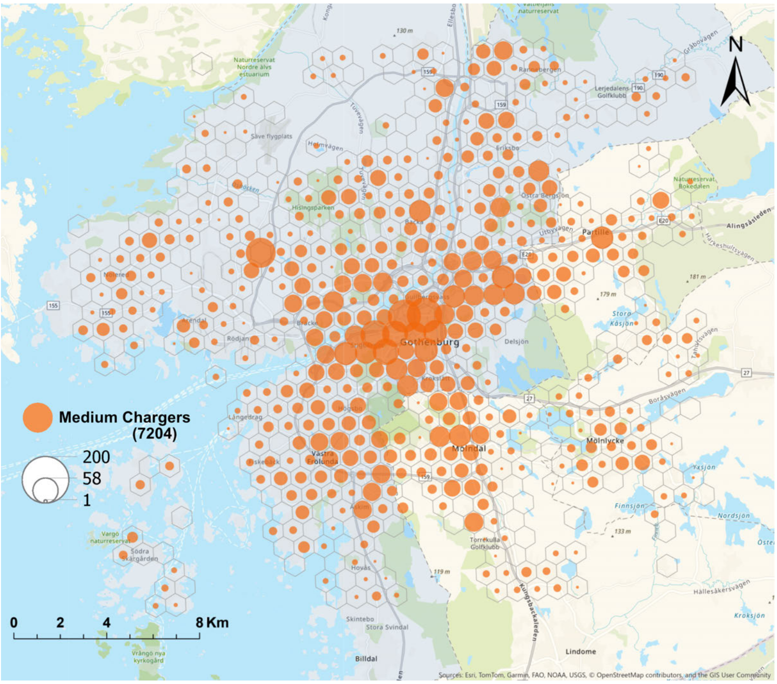

(b) Medium Charger counts per hex-grid cell for the study region

Figure 4.12: Spatial distribution of Public EV chargers in Gothenburg region.

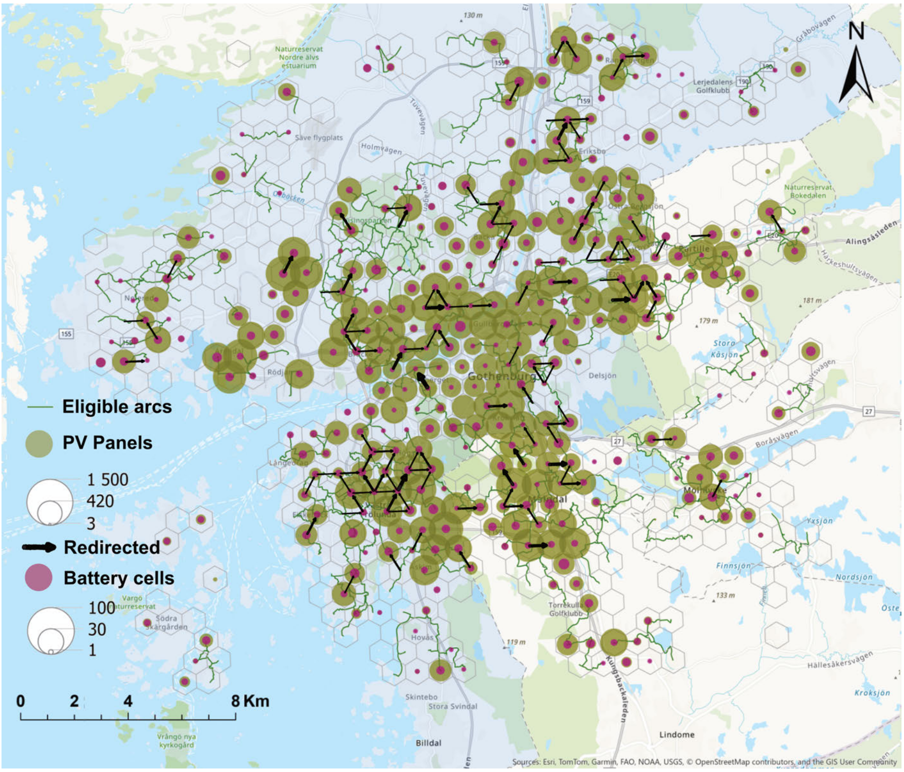

Figure 4.13: June representative day PV (green), BESS (blue), and redirection flows (arrows).

the evening back toward 20%. All SoC paths remain within the 10-90% bounds, confirming durability and responsiveness without excessive cycling.

4.3.5 Spatial user redirection dynamics

Spatial demand redirection emerges as a powerful complement to temporal load management, leveraging user redirection incentives to smooth peak charging demand and maximize renewable utilization. Figure 4.13 illustrates, for June representative day, how the model superimposes optimal PV panel and BESS deployments with the highest-value redirection arcs (within the 1.5 km travel radius). The effectiveness of each redirection arc depends on three concurrent factors. The destination cell's surplus of low-cost renewable or stored energy, the local retail tariff exceeding the combined marginal energy cost plus the travel-time rebate, and the driver's willingness to detour under the distance threshold. Midday hours, when ToU tariffs approach 2.0 SEK/kWh and PV capacity factors peak, consistently yield the greatest net incentive rents, triggering the majority of profitable rerouting (Figure 4.15).

Seasonal sensitivity is stark. In July, despite similarly high solar output

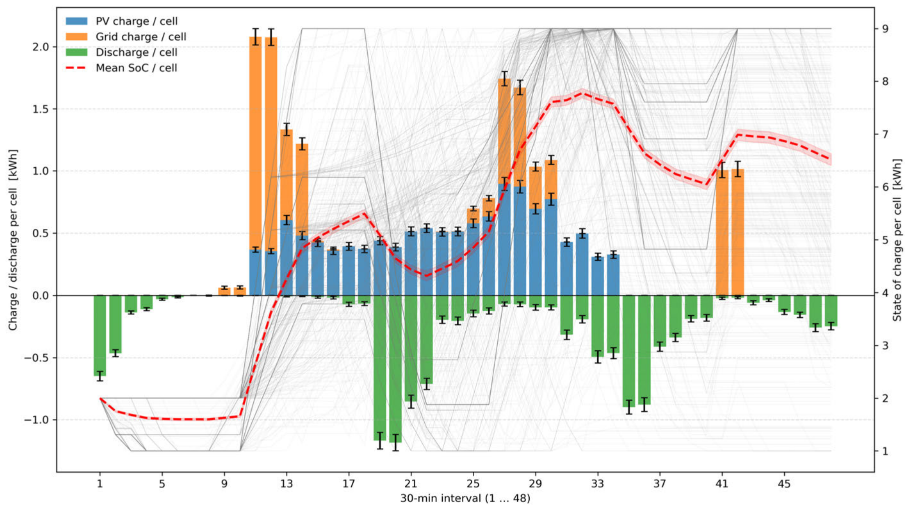

Figure 4.14: Optimal Battery scheduling operations (January representative day)

(over 0.8 capacity factor), a 25% drop in retail tariffs erodes price margins below incentive thresholds, collapsing redirected volumes (near zero). Conversely, in September, recovering tariffs (up to 1.9 SEK/kWh) cannot compensate for low PV generation (up to 0.55 capacity factor), so redirections occur only when and where residual renewable surplus exists, limiting daily opportunities to a few critical hours. BESS further amplifies user redirection potential by time-shifting PV energy into high-tariff windows. In summer months, up to 12% of redirected demand originates from BESS discharge. By autumn, this share rises toward 25%, reflecting reduced daylight and greater reliance on stored energy. The combined PV+BESS infrastructure thus broadens profitable redirection windows well beyond raw solar peaks. Over an entire year, redirected demand of 0.93 GWh (Table 4.5) incurs SEK 5.11 million in rebates but offsets high-tariff grid purchases and defers the need for incremental fast chargers during afternoon peaks. Although this redirected energy represents under 1% of total delivered kWh, its impact on operating profits, particularly on high PV days, is disproportionately large, underscoring the strategic value of spatial flexibility. Policy levers also emerge. A modest 0.2 SEK/kWh uplift in tariffs of July would unlock latent PV potential, multiplying redirected volumes without new capital outlay. Alternatively, temporarily lowering distance-based incentives during tariff-depressed months could sustain redirection economics without harming consumer welfare. Overall, the spatial redirection mechanism, which couples per-kWh travel-time rebates with fine-grained infrastructure and renewable placement, proves a robust tool for peak shaving and renewable integration. Its success, however, hinges on the precise alignment of tariff schedules, weather-driven PV availability, and thoughtfully sited PV+BESS assets.

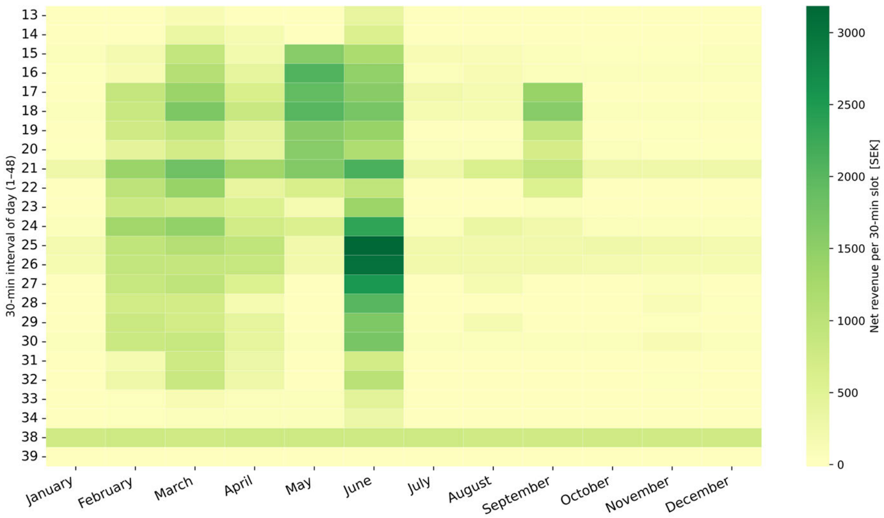

Figure 4.15: Monthly-interval net revenue (SEK/kWh) from redirected charging.

4.3.6 Local insights: Mölnlycke suburban node

Figure 4.16 zooms in on a representative suburban fringe cell in Mölnlycke (see Figure 4.1). Figure 4.16 (a) depicts the hourly profile of total charging demand, peaking sharply during the 17:00-19:00 commuter return window. Figure 4.16 (b) shows that only a small fraction of this demand is met by private home chargers, reflecting the area's lower residential density and limited private-charger penetration. Consequently, Figure 4.16 (c) reveals substantial public charging demand throughout the daytime, especially along the adjacent transport corridor where through-traffic and transit stops generate residual load once home charging is exhausted. In response, the optimization locates public chargers in the eastern and southern hexagons surrounding Mölnlycke's core. Marshland, lakes, and fractured road connectivity limit feasible redirection to under 0.9 km, well below our 1.5 km cap (Equation (3.23)), necessitating more local bays. Figure (d) overlays optimal PV panel clusters (200-400 panels per cell) and small-scale BESS deployments (up to 10 units), sited along arterial corridors with both rooftop-PV potential and low grid expansion costs. June's redirection flows (arrows) emanate during the 16:00-18:00 peak from central Mölnlycke toward these renewable-rich outskirts, confirming that drivers elect to detour when the destination cell offers cost savings via on-site solar or stored energy.

These patterns illustrate the fidelity of our MILP framework in aligning charger siting with local land cover, network topology, and demand vectors. In Mölnlycke, where private-charger access is sparse and redirection distances are constrained, the model invests in medium- and fast-speed public chargers to meet peak needs. Conversely, where connectivity and solar availability allow, it

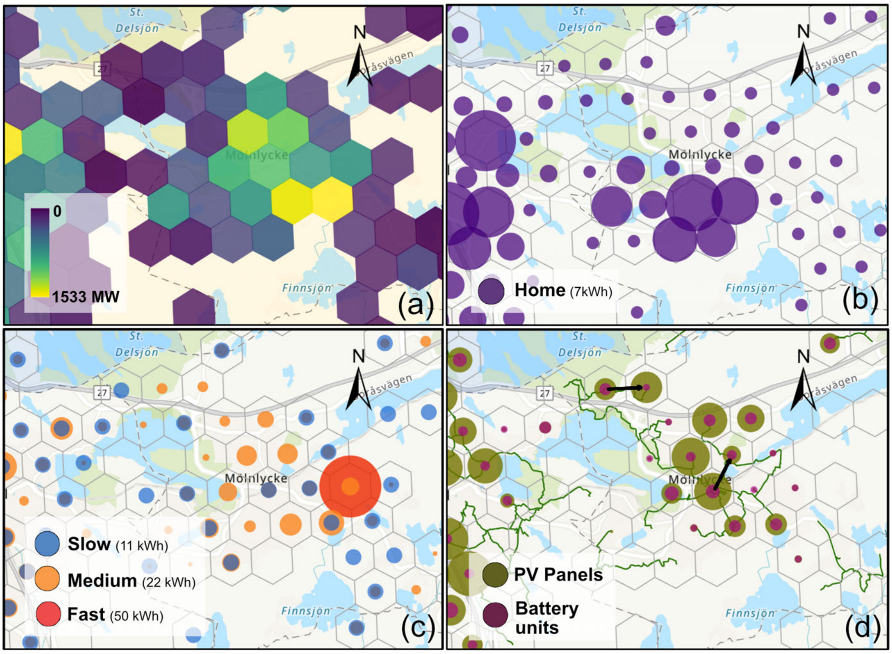

Figure 4.16: Local Insights for Mölnlycke area outside Gothenburg (a) Annual charging demands (b) Home demand (c) Public demand (d) PV panels, BESS and redirections

favors smaller public sites augmented by PV and BESS, enabling economically viable redirection and reduced reliance on the main grid.

4.3.7 Carbon emission reduction

To quantify the climate benefits of co-locating PV and BESS (Scenario 3) versus the grid-only baseline, we calculate avoided operational CO_2 emissions by replacing grid procurement with local renewables and storage dispatch. Adopting Sweden's 2024 average grid factor of 9 g CO_2e /kWh, we multiply each half-hour's PV-to-charger and PV-to-battery-to-charger energy by this factor and aggregate monthly via representative-day scaling ($N_{\text{days}}(m)$):

$$\Delta E_{\text{annual}} = \sum_{m \in \mathcal{M}} \sum_{t \in \mathcal{H}} N_{\text{days}}(m)\, \eta_{\text{grid}} \Big(E_{m,t}^{\text{PV}\to\text{char}} + E_{m,t}^{\text{PV}\to\text{batt}\to\text{char}} \Big).$$

Using Scenario 3's dispatch results, the model avoids roughly 317.3 t CO_2e per year. On a representative summer day (June), total savings reach 1 455.6 kg CO_2e: 1 376.5 kg from direct PV charging and 79 kg via stored PV discharge. Figure 4.17 presents a monthly × half-hour heatmap of avoided emissions (kg CO_2e per interval). Peak reductions occur during mid-day to late afternoon

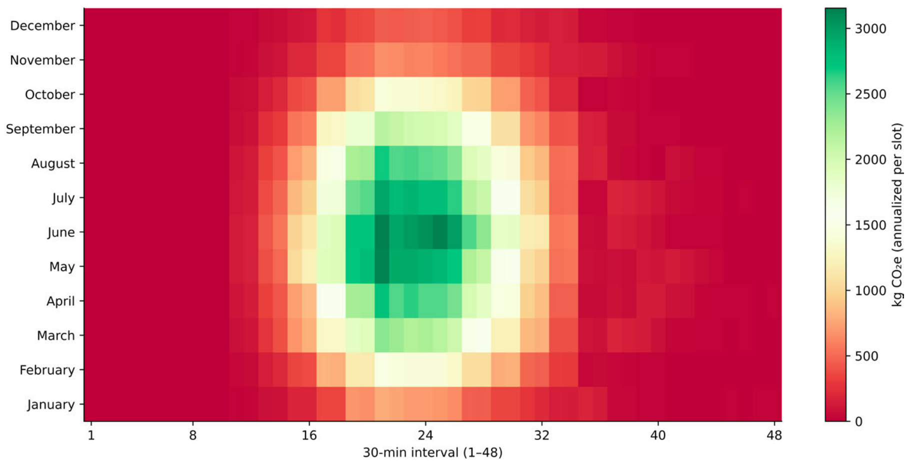

Figure 4.17: Heatmap of avoided CO_2e emissions (kg per half-hour) under Scenario 3 vs. baseline.

(intervals 16-30) in May-July, mirroring the highest PV capacity factors and reinforcing the compatibility between solar availability and carbon savings.

These results demonstrate that integrating on-site renewables and storage not only boosts CPO profitability but also delivers meaningful environmental gains. By shifting up to a quarter of midday load onto zero-carbon PV and strategically discharging batteries during high-tariff intervals, the optimized infrastructure achieves both peak-shaving and an annual reduction of approximately 320 t CO_2e. This dual economic-environmental benefit emphasizes the value of combining RES deployment with demand-management incentives in urban EV charging networks.

As demonstrated here, from high resolution, behaviorally enriched demand simulation in MATSim to the holistic MILP co-optimization of chargers, renewables, storage, and spatial incentives, yields a coherent, city wide blueprint for EV infrastructure planning in Gothenburg. These results not only capture the nuanced interplay of user choices, tariff signals, and renewable availability at the urban scale but also illustrate a methodology that can readily be extended to national or multi-regional contexts, provided the requisite demographic, network, and market data alongside sufficient computational resources. Nevertheless, our present analysis abstracts away certain real-world complexities, most notably distribution grid reliability and feeder-level power flows, which can critically affect both the feasibility and the economic performance of large-scale deployments. In the following Chapter 5, we critically reflect on these limitations, outline the necessary enhancements, and chart a roadmap for future research to further strengthen the robustness and applicability of this end-to-end electrification framework.

Chapter 5

Conclusion and Discussions

This chapter summarizes the key findings from this thesis including a behaviorally rich agent-based charging demand model (Chapter 3) and a large-scale mixed-integer optimization of charging infrastructure, co-located photovoltaic (PV) generation, battery energy storage systems (BESS), and user redirection incentives (Chapter 3). The summary is structured to highlight (i) the methodological advances, (ii) major empirical insights from the Gothenburg case study, (iii) cross-cutting implications for policy and practice, and (iv) limitations and future research pathways.

The extended MATSim-based agent-based model explicitly incorporates *cost-aware and adaptive charging behavior*, allowing agents to respond to ToU tariffs, battery state-of-charge SoC, and heterogeneous charging access constraints. This enables the endogenous emergence of charging events, both *event-triggered* SoC threshold) and *plan-ahead* (cost-minimising) strategies, within the co-evolutionary replanning process. On the supply side, the optimization framework jointly considers charger siting and sizing (across slow, medium, and fast chargers), PV and BESS deployment, dynamic BESS scheduling, and spatial user redirection. The model operates at high spatiotemporal granularity, half-hourly intervals, monthly representative days, capturing seasonal solar variability and demand patterns. Unlike most optimization studies, this thesis embeds a user-incentive mechanism for spatial redirection of charging demand. Redirection arcs are constrained by realistic travel time and distance thresholds, available charger capacity at the destination, and economic acceptability from the users perspective. This formulation captures both the operational feasibility and the behavioral plausibility of demand-side measures.

5.1 Spatiotemporal charging demand dynamics in Gothenburg

The Gothenburg case study, evaluated under a 50% EV penetration scenario, demonstrates pronounced temporal and spatial variation in charging demand patterns. Home charging constitutes the dominant share during the overnight period and around midday, whereas workplace charging peaks sharply during the morning commute. Public charging displays a more consistent profile throughout the day, with concentrations in high-density urban districts.

In the *non-cost aware* baseline scenario, the arrival of vehicles at workplaces in the morning produces pronounced demand peaks. When price awareness is introduced, a substantial portion of daytime charging shifts from workplace to home locations, particularly into the low tariff overnight window. Adaptive smart charging behaviors further flatten the evening residential peak, reducing it by as much as 15%, while increasing off-peak charging volumes without significantly impairing daytime accessibility. These dynamics underscore the need to account for behavioral responses to price signals and technical flexibility measures when planning charging infrastructure and grid operations. The detailed analysis of charging demand dynamics yields the following specific insights:

- Incorporating dynamic ToU tariffs into the charging demand estimation causes a notable reallocation of energy demand from daytime workplace locations to homes, yet the dominant evening system peak remains largely intact. This finding highlights the importance of reflecting tariff structures in modeling, as their omission can lead to incorrect estimation of spatiotemporal demand profiles.
- Introducing probabilistic smart charging behavior substantially reshapes the demand curve, lowering the home charging peak between 17:00 and 22:00 hours by up to 11% and reallocating roughly 20% of residential charging energy to the low-cost overnight period.
- Significant heterogeneity is observed in charging strategies among agents with otherwise identical travel schedules. Differences in location-specific tariffs and adaptive charging decisions lead to diverse strategies for cost minimization. This diversity reinforces the value of embedding behavioral variation and cost-awareness into spatiotemporal demand estimation.
- Spatial and temporal demand patterns vary widely across the city. For instance, central Gothenburg districts such as Inom Vallgraven exceed 20 MWh/day, almost triple the daily energy observed in peripheral areas like Surte. Workplace charging demand in the city core peaks at approximately 7 MWh at 08:00 hours, whereas suburban demand is dominated by off-peak home charging volumes below 1.1 MWh. Such disparities emphasize the necessity of agent-based approaches that jointly capture spatial and temporal influences on user charging behavior.

Overall, the modeling results present a behaviorally detailed and spatially explicit picture of charging needs in an urban EV transition context. The outcomes highlight both opportunities for peak reduction through smart charging and the limitations of relying solely on tariff adjustments to manage demand. These findings form a robust basis for the optimization stage of the pipeline, where infrastructure siting, sizing, and operational strategies can be tailored to the observed behavioral and spatial heterogeneity.

5.2 Impact of integrated PV, BESS, and user redirection

The optimization analysis for the Gothenburg 50% EV penetration scenario demonstrates that the combined deployment of PV, BESS, and spatially targeted user redirection strategies substantially improves both operational performance and economic outcomes compared to a charger-only baseline. By explicitly integrating high resolution charging demand profiles from MATSim with land-use capacity limits, dynamic ToU tariffs, and travel-time based incentive mechanisms, the framework quantifies how distributed renewable generation and storage, together with behavioral demand management, can be co-optimized to enhance profitability while reducing grid dependence.

The integrated approach delivers measurable benefits across cost savings, renewable utilization, and emissions reduction. The results indicate that, beyond increasing operator profit margins, such a configuration improves the resilience of the charging network by flattening daily load profiles and better matching supply from distributed RES to demand peaks. Importantly, this synergy is most pronounced when BESS and PV are co-located in high demand zones and linked to underutilized capacity via user redirection incentives.

The key quantitative findings are as follows:

- The combined integration of PV, BESS, and user redirection yields an annual net profit increase of approximately SEK 31.5 million (+2.25%) relative to the optimal charger-only configuration. PV generation alone offsets around 35.5 GWh/year of grid electricity purchases, producing annual procurement cost savings exceeding SEK 35 million.
- Substituting grid electricity with local PV output and BESS-stored energy avoids roughly 320 tCO_2e per year, with the largest emissions reductions occurring during summer midday peaks when PV capacity factors exceed 75% of their theoretical maximum.
- In the optimized infrastructure portfolio, medium-speed (22 kW) chargers dominate due to their cost-effectiveness and alignment with typical dwell times, representing more than 95% of public units. Fast DC (50 kW) chargers are deployed only at high value arterial nodes and park-and-ride facilities, while slow AC (11 kW) chargers are used to fill accessibility gaps in suburban and peri-urban areas.

- PV installations are concentrated in high demand urban zones where sufficient surface area is available, ensuring that most generated energy is consumed locally. BESS units are co-located with PV arrays and placed near centralized demand clusters to maximize both tariff-arbitrage potential and daily load smoothing.

- The presence of BESS extends the effective time window for profitable user redirection by enabling evening discharge from midday PV surpluses. In the fully integrated scenario, redirected demand exceeds 0.9 GWh/year, more than eight times higher than in cases without PV, thereby reducing the need for additional high-capacity chargers in overloaded cells and increasing renewable electricity utilization.

Overall, the modeling confirms that co-locating public charging with distributed PV and BESS, and coupling this with strategically incentivised demand redirection, creates a more profitable, sustainable, and operational charging ecosystem. Such configurations attenuate peak loads, reduce reliance on high-cost grid electricity, and contribute directly to climate goals through avoided emissions. While the present formulation uses a representative day approach to capture seasonal variability with lower computational cost, future extensions could incorporate explicit feeder-level grid constraints, stochastic renewable generation and demand variability, and charger type differentiation in redirection flows. Such enhancements would further align the optimization outputs with real-world operational requirements and increase the transferability of these findings to other urban contexts.

5.3 Study Implications and Practicality

The results confirm that integrating distributed PV and BESS with behaviorally informed demand management can significantly reduce reliance on the central grid during peak-tariff periods, alleviating stress on vulnerable distribution network nodes. By capturing behavioral diversity and price responsiveness, the framework avoids over provisioning of high-cost fast chargers in locations where demand can be economically redirected. This enables more balanced infrastructure investment, aligning public charging capacity with actual utilization potential. The methodology is inherently scalable to larger geographies and higher penetration levels, provided suitable data are available. Its modular structure allows adaptation to other urban contexts, differing policy environments, and alternative renewable or storage technologies.

Key limitations of this work include the aggregate representation of grid interactions, where the optimization operates at a regional level without explicitly modeling low-voltage feeder constraints. The exclusion of vehicle-to-grid (V2G) services represents another constraint, as incorporating bidirectional charging could potentially enhance system flexibility and enable additional revenue streams. behavioral parameters, although calibrated using relevant literature, remain subject to uncertainty, particularly regarding long-term adoption of smart charging technologies and heterogeneous user responses to dynamic tariffs. Furthermore, both PV generation and charging demand are treated deterministically for each representative day, which limits the ability to assess robustness under weather variability or unexpected demand fluctuations. Future research could address these gaps by coupling the planning framework with detailed power flow models to evaluate feeder-level constraint violations and hosting capacity limits. Incorporating V2G and broader bidirectional charging economics would enable more comprehensive assessments of flexibility potential. Extending behavioral modeling to capture long-term adoption trajectories and varied responses to emerging tariff structures would improve realism, while stochastic optimization approaches could better account for uncertainties in renewable generation, electricity prices, and charging demand patterns across seasons and years.

This thesis demonstrates that combining behaviorally realistic charging demand estimation with co-optimized deployment of charging infrastructure, PV generation, and storage, augmented by incentive-based user redirection, can deliver substantial operational, economic, and environmental benefits for urban e-mobility systems. The Gothenburg case study shows that strategic integration of renewable generation and demand flexibility measures not only mitigates grid impacts but also enhances profitability and sustainability. The proposed framework thus offers a transferable, evidence-based decision-support tool for planners and operators navigating the transition to large-scale electric mobility.

Appendix A

Nomenclature

A.1 Extended MATSim framework

S^*_{plan}	Baseline plan score combining activity and travel utilities over all segments.
N	Number of tour segments in a daily plan.
$S_{\text{act},q}$	Utility of performing activity q (duration benefit & early/late penalties).
$t_{\text{dur},q}$, $t_{\text{dur},0}$	Actual and reference durations of activity q.
β_{dur}, β_{early}, β_{late}	Marginal utility of duration; early and late schedule penalties.
$S_{\text{trav},q}$	Disutility of the travel leg q (mode, time, money, distance, transfers).
$C_{\text{mode}(q)}$	Mode-specific constant disutility for leg q.
$t_{\text{trav},q}$, $d_{\text{trav},q}$	Travel time and distance for leg q.
$\beta_{\text{trav},\text{mode}(q)}$, $\beta_{d,\text{mode}(q)}$, $\gamma_{d,\text{mode}(q)}$, β_m, β_{transfer}	Marginal disutilities for travel time, distance, money, and transfers.
Δm_q, $x_{\text{transfer},q}$	Monetary cost and number of transfers in leg q.
$S_{\text{EV,plan}}$	EV-augmented plan score including charging costs and penalties.
β_{money}, $\beta_{\text{rangeAnxiety}}$, $\beta_{\text{emptyBattery}}$, β_{walking}, β_{SoCdiff}	Marginal utilities for charging cost, range anxiety, depletion, walking, and SoC deviation.

$c_{\text{charging}}(t)$	Instantaneous charging cost at time t (kWh $\times$ tariff).
$M_{\text{temporal}}(t)$	Time-of-use multiplier for charging cost at hour corresponding to t.
$S_{\text{rangeAnxiety}}$, $S_{\text{emptyBattery}}$	Disutility terms for low SoC and fully depleted battery.
S_{walking}	Walking disutility to charger: $1-\exp(-\lambda\, d_{\text{walk}}/d_{\text{walk,max}})$.
S_{SoCdiff}	Penalty proportional to $(\text{SoC}_{\text{start}} - \text{SoC}_{\text{end}})$.
$t_{\text{start}}^{\text{opt}}$	Optimal charging start time within $[t_{\text{arr}},\, t_{\text{dep}} - T_{\text{charge}}]$.
λ, λ_{walk}, $thres_{\text{SoC}}$, T_{charge}	Exponential decay rate; max walk distance; SoC threshold; required charging duration.

A.2 MILP Optimization formulation

(a) Sets and Indices

$i \in \mathcal{I}$	Hex-cell index and set of potential sites.
$m \in \mathcal{M}$	Month index and set, $\{\text{Jan}, \ldots, \text{Dec}\}$.
$t \in \mathcal{H}$	Half-hour interval index and set, $\{1, \ldots, 48\}$.
$b \in \mathcal{B}$	Demand class, $\{\text{home}, \text{public}\}$.
$c \in \mathcal{C}$	Public charger type, $\{\text{slow}, \text{medium}, \text{fast}\}$.
$(i, j) \in \mathcal{D}$	Potential redirection arc between cells within $d_{\max}$.
$(i, j, m, t) \in \mathcal{A}$	Active redirection arc at $(i \to j)$ when the demand threshold is met.

(b) Parameters

$N_{\text{days}}(m)$	Representative days in month m.
DAYS	Total days in planning horizon (annual = 365).
$\overline{C}_i^{\text{pub}}$	Max public chargers at cell i.
$\overline{C}_i^{\text{home}}$	Exogenous home chargers at cell i.
K_c	kWh capacity per interval of charger c.
ρ^c	Daily annuity cost of charger c (SEK/day).

$\overline{\Psi}_i$	Max PV panels at cell i.
Ψ^{cap}	kWh output per PV panel per interval.
$p^{\text{pv}}_{m,t}$	PV availability factor in (m, t).
$\overline{\Theta}_i$	Max battery units at cell i.
Cap^{Θ}	kWh capacity per battery unit.
$\eta_{\text{ch}}, \eta_{\text{dis}}$	charge-discharge efficiencies.
$\rho_{m,t}$	Retail electricity price in (m, t) (SEK/kWh).
Price_c	Charging tariff at charger c (SEK/kWh).
$T_{i,j}$	Incentive rebate (SEK/kWh) for redirecting from i to j.
λ_{slack}	Penalty per unmet kWh.
κ	kWh per redirected trip.
$\kappa_{\min}$	Min kWh to activate an arc.
τ	Intervals per hour.
$\alpha, \beta_{\min}, \beta_{\max}$	Initial, min, max SoC fraction.
$d_{\max}$	Max network distance for redirection.

(c) Decision Variables

$x_{i,c} \in \mathbb{Z}_+$	Count of public chargers of type c at cell i.
$\Psi_i \in \mathbb{Z}_+$	Count of PV panels at cell i.
$\Theta_i \in \mathbb{Z}_+$	Count of battery units at cell i.
$e_{i,m,t,c,b} \geq 0$	kWh delivered by charger c to class b.
$g^{\text{dir}}_{i,m,t,b} \geq 0$	Direct grid supply to class b.
$g^{\text{batt}}_{i,m,t} \geq 0$	Grid$\rightarrow$battery kWh.
$p^{\text{batt}}_{i,m,t} \geq 0$	PV$\rightarrow$battery kWh.
$d^{\text{dis}}_{i,m,t,b} \geq 0$	Battery discharge to class b.
$\chi_{i,m,t} \geq 0$	State-of-charge (kWh).
$\epsilon_{i,m,t,b} \geq 0$	Unmet demand slack.
$z_{i,j,m,t} \geq 0$	kWh redirected from i to j.
$n^{\kappa}_{i,j,m,t} \in \mathbb{Z}_+$	Count of redirected trips $(i \rightarrow j)$.
$Y_{i,j,m,t} \in \{0, 1\}$	Arc-activation flag.
$\delta_{i,m,t} \in \{0, 1\}$	Battery charge-discharge mode.

Bibliography

Abdullah, H.M., Gastli, A., Ben-Brahim, L., Mohammed, S.O., 2022. Integrated Multi-Criteria Model for Long-Term Placement of Electric Vehicle Chargers. IEEE Access 10, 123452–123473. doi:10.1109/ACCESS.2022.3224796.

Adenaw, L., Lienkamp, M., 2021. Multi-Criteria, Co-Evolutionary Charging Behavior: An Agent-Based Simulation of Urban Electromobility. World Electric Vehicle Journal 12, 18. doi:10.3390/wevj12010018.

Ahmad, F., Iqbal, A., Ashraf, I., Marzband, M., Khan, I., 2022. Optimal location of electric vehicle charging station and its impact on distribution network: A review. Energy Reports 8, 2314–2333. doi:10.1016/j.egyr.2022.01.180.

Alvarez Guerrero, J.D., Acker, T.L., Castro, R., 2022. Power System Impacts of Electric Vehicle Charging Strategies. Electricity 3, 297–324. doi:10.3390/electricity3030017.

Ameur, A., Berrada, A., Loudiyi, K., Aggour, M., 2020. Forecast modeling and performance assessment of solar PV systems. Journal of Cleaner Production 267, 122167. doi:10.1016/j.jclepro.2020.122167.

Arabani, H.P., Ingelström, M., Márquez-Fernández, F.J., Alaküla, M., 2024. Electric Road Systems for Electric Vehicle Long-Distance Travel: A Multi-Agent Simulation Approach, in: 2024 IEEE International Conference on Electrical Systems for Aircraft, Railway, Ship Propulsion and Road Vehicles & International Transportation Electrification Conference (ESARS-ITEC), IEEE, Naples, Italy. pp. 1–6. doi:10.1109/ESARS-ITEC60450.2024.10819876.

Arias, M.B., Bae, S., 2016. Electric vehicle charging demand forecasting model based on big data technologies. Applied Energy 183, 327–339. doi:10.1016/j.apenergy.2016.08.080.

Arslan, O., Karaşan, O.E., 2016. A Benders decomposition approach for the charging station location problem with plug-in hybrid electric vehicles. Transportation Research Part B: Methodological 93, 670–695. doi:10.1016/j.trb.2016.09.001.

Banol Arias, N., Tabares, A., Franco, J.F., Lavorato, M., Romero, R., 2018. Robust Joint Expansion Planning of Electrical Distribution Systems and EV Charging Stations. IEEE Transactions on Sustainable Energy 9, 884–894. doi:10.1109/TSTE.2017.2764080.

Bian, C., Li, H., Wallin, F., Avelin, A., Lin, L., Yu, Z., 2019. Finding the optimal location for public charging stations – a GIS-based MILP approach. Energy Procedia 158, 6582–6588. doi:10.1016/j.egypro.2019.01.071.

Bibak, B., Tekiner-Mogulkoc, H., 2021. Influences of vehicle to grid (V2G) on power grid: An analysis by considering associated stochastic parameters explicitly. Sustainable Energy, Grids and Networks 26, 100429. doi:10.1016/j.segan.2020.100429.

Birk Jones, C., Vining, W., Lave, M., Haines, T., Neuman, C., Bennett, J., Scoffield, D.R., 2022. Impact of Electric Vehicle customer response to Time-of-Use rates on distribution power grids. Energy Reports 8, 8225–8235. doi:10.1016/j.egyr.2022.06.048.

Bouhouras, A.S., Kothona, D., Gkaidatzis, P.A., Christoforidis, G.C., 2022. Distribution network energy loss reduction under ev charging schedule. International Journal of Energy Research 46, 8256–8270. doi:10.1002/er.7727.

Brouwer, A.S., Kuramochi, T., Van Den Broek, M., Faaij, A., 2013. Fulfilling the electricity demand of electric vehicles in the long term future: An evaluation of centralized and decentralized power supply systems. Applied Energy 107, 33–51. doi:10.1016/j.apenergy.2013.02.005.

Calazans Campelo, C.E., Bertolotto, M., Corcoran, P., Dey, N. (Eds.), 2017. Volunteered Geographic Information and the Future of Geospatial Data:. Advances in Geospatial Technologies, IGI Global. doi:10.4018/978-1-5225-2446-5.

Casini, M., Vicino, A., Zanvettor, G.G., 2021. A receding horizon approach to peak power minimization for EV charging stations in the presence of uncertainty. International Journal of Electrical Power & Energy Systems 126, 106567. doi:10.1016/j.ijepes.2020.106567.

Cavalcante, I., Rodrigues da Silva, A., Zajc, M., Mendek, I., Calearo, L., Malkova, A., Ziras, C., Pediaditis, P., Michos, K., Mateus, J., Matias, S., Brito, M., Lekidis, A., Guzman, C.P., Nunes, A.R., Morais, H., 2024. Dataset on Electric Road Mobility: Historical and Evolution Scenarios until 2050. Scientific Data 11, 1019. doi:10.1038/s41597-024-03801-3.

Chauhan, B., Jain, S.K., 2024. Scheduling of Electric Vehicle's Power in V2G and G2V Modes Using an Improved Charge–Discharge Opportunity-Based Approach. IEEE Transactions on Transportation Electrification 10, 811–822. doi:10.1109/TTE.2023.3265681.

Christensen, K., Ma, Z., Jørgensen, B.N., 2024. Multi-agent Based Simulation for Investigating Electric Vehicle Adoption and Its Impacts on Electricity Distribution Grids and CO2 Emissions, in: Jørgensen, B.N., Da Silva, L.C.P., Ma, Z. (Eds.), Energy Informatics. Springer Nature Switzerland, Cham. volume 14468, pp. 3–19. doi:10.1007/978-3-031-48652-4_1. series Title: Lecture Notes in Computer Science.

Csiszár, C., Csonka, B., Földes, D., Wirth, E., Lovas, T., 2019. Urban public charging station locating method for electric vehicles based on land use approach. Journal of Transport Geography 74, 173–180. doi:10.1016/j.jtrangeo.2018.11.016.

Cui, S., Zhao, N., 2024. A Study on the Current Status and Future Prospects of EV Automotive Market. Journal of Social Science and Cultural Development 1. doi:10.70767/jsscd.v1i2.296.

Dai, Q., Liu, J., Wei, Q., 2019. Optimal Photovoltaic/Battery Energy Storage/Electric Vehicle Charging Station Design Based on Multi-Agent Particle Swarm Optimization Algorithm. Sustainability 11, 1973. doi:10.3390/su11071973.

Daniels, R., Mulley, C., 2013. Explaining walking distance to public transport: The dominance of public transport supply. Journal of Transport and Land Use 6, 5–20. doi:10.5198/jtlu.v6i2.308.

Das, J., K, V., Daniel, J., 2022. Prediction of Electric Vehicle Charging Load with Uncertainty using Probabilistic Methodology, in: 2022 IEEE International Power and Renewable Energy Conference (IPRECON), IEEE, Kollam, India. pp. 1–5. doi:10.1109/IPRECON55716.2022.10059502.

Deb, S., Tammi, K., Kalita, K., Mahanta, P., 2018a. Impact of Electric Vehicle Charging Station Load on Distribution Network. Energies 11, 178. doi:10.3390/en11010178.

Deb, S., Tammi, K., Kalita, K., Mahanta, P., 2018b. Review of recent trends in charging infrastructure planning for electric vehicles. WIREs Energy and Environment 7, e306. doi:10.1002/wene.306.

Dey, B., Krishnamurthy, S., Fose, N., Ratshitanga, M., Moodley, P., 2024. A Metaheuristic Approach to Analyze the Techno-Economical Impact of Energy Storage Systems on Grid-Connected Microgrid Systems Adapting Load-Shifting Policies. Processes 13, 65. doi:10.3390/pr13010065.

Dong, X.J., Shen, J.N., Liu, C.W., Ma, Z.F., He, Y.J., 2024. Simultaneous capacity configuration and scheduling optimization of an integrated electrical vehicle charging station with photovoltaic and battery energy storage system. Energy 289, 129991. doi:10.1016/j.energy.2023.129991.

Duan, M., Liao, F., Qi, G., Guan, W., 2023. Integrated optimization of electric bus scheduling and charging planning incorporating flexible charging and timetable shifting strategies. Transportation Research Part C: Emerging Technologies 152, 104175. doi:10.1016/j.trc.2023.104175.

Ensslen, A., Ringler, P., Dörr, L., Jochem, P., Zimmermann, F., Fichtner, W., 2018. Incentivizing smart charging: Modeling charging tariffs for electric vehicles in German and French electricity markets. Energy Research & Social Science 42, 112–126. doi:10.1016/j.erss.2018.02.013.

Erbaş, M., Kabak, M., Özceylan, E., Çetinkaya, C., 2018. Optimal siting of electric vehicle charging stations: A GIS-based fuzzy Multi-Criteria Decision Analysis. Energy 163, 1017–1031. doi:10.1016/j.energy.2018.08.140.

Ermagun, A., Tian, J., 2024. Charging into inequality: A national study of social, economic, and environment correlates of electric vehicle charging stations. Energy Research & Social Science 115, 103622. doi:10.1016/j.erss.2024.103622.

ETH Zürich, Waraich, R.A., Bischoff, J., TU Berlin, 2016. Electric Vehicles, in: ETH Zürich, Horni, A., Nagel, K., TU Berlin (Eds.), The Multi-Agent Transport Simulation MATSim. Ubiquity Press, pp. 93–96. doi:10.5334/baw.14.

European Commission. Joint Research Centre., 2023. Distribution system operator observatory 2022: managing innovation and RES grid connection for a carbon neutral Europe. Publications Office, LU. URL: https://data.europa.eu/doi/10.2760/778963.

European Commission. Joint Research Centre., 2025. Photovoltaics geographical information system: status report 2024. Publications Office, LU. URL: https://data.europa.eu/doi/10.2760/2979595.

Fachrizal, R., Qian, K., Lindberg, O., Shepero, M., Adam, R., Widén, J., Munkhammar, J., 2024. Urban-scale energy matching optimization with smart EV charging and V2G in a net-zero energy city powered by wind and solar energy. eTransportation 20, 100314. doi:10.1016/j.etran.2024.100314.

Fadranski, D., Syré, A.M., Grahle, A., Göhlich, D., 2023. Analysis of Charging Infrastructure for Private, Battery Electric Passenger Cars: Optimizing Spatial Distribution Using a Genetic Algorithm. World Electric Vehicle Journal 14, 26. doi:10.3390/wevj14020026.

Fayyaz S., S.K., Liu, X.C., Zhang, G., 2017. An efficient General Transit Feed Specification (GTFS) enabled algorithm for dynamic transit accessibility analysis. PLOS ONE 12, e0185333. doi:10.1371/journal.pone.0185333.

Formolli, M., Kleiven, T., Lobaccaro, G., 2023. Assessing solar energy accessibility at high latitudes: A systematic review of urban spatial domains, metrics, and parameters. Renewable and Sustainable Energy Reviews 177, 113231. doi:10.1016/j.rser.2023.113231.

Gairola, P., Nezamuddin, N., 2023. Optimization framework for integrated battery electric bus planning and charging scheduling. Transportation Research Part D: Transport and Environment 118, 103697. doi:10.1016/j.trd.2023.103697.

Garrison, A., Rashid, M., Chen, N., 2023. A Synergistic Learning Based Electric Vehicle Charging Demand Prediction Scheme, in: SoutheastCon 2023, IEEE, Orlando, FL, USA. pp. 5–10. doi:10.1109/SoutheastCon51012.2023.10115078.

Ghania, S.M., Mahmoud, K.R.M., Hashmi, A.M., 2022. Reliability Study of Renewable Energy Resources and their Integration with Utility Grids. Engineering, Technology & Applied Science Research 12, 9078–9086. doi:10.48084/etasr.5090.

Giménez-Gaydou, D.A., Ribeiro, A.S.N., Gutiérrez, J., Antunes, A.P., 2016. Optimal location of battery electric vehicle charging stations in urban areas: A new approach. International Journal of Sustainable Transportation 10, 393–405. doi:10.1080/15568318.2014.961620.

Goh, H.H., Zong, L., Zhang, D., Liu, H., Dai, W., Lim, C.S., Kurniawan, T.A., Teo, K.T.K., Goh, K.C., 2022. Mid- and long-term strategy based on electric vehicle charging unpredictability and ownership estimation. International Journal of Electrical Power & Energy Systems 142, 108240. doi:10.1016/j.ijepes.2022.108240.

Göberndorfer, L., Savanovic, M., Jäger, G., 2024. Charging Rush Hour: Modeling Peak Electricity Demand for Charging a Fully Electric Fleet. Sage Open 14, 21582440241290044. doi:10.1177/21582440241290044.

Hartvigsson, E., Taljegard, M., Odenberger, M., Chen, P., 2022. A large-scale high-resolution geographic analysis of impacts of electric vehicle charging on low-voltage grids. Energy 261, 125180. doi:10.1016/j.energy.2022.125180.

He, S., Luo, S., Sun, K.K., 2022. Factors affecting electric vehicle adoption intention: The impact of objective, perceived, and prospective charger accessibility. Journal of Transport and Land Use 15, 779–801. doi:10.5198/jtlu.2022.2113.

Hu, J., Morais, H., Sousa, T., Lind, M., 2016. Electric vehicle fleet management in smart grids: A review of services, optimization and control aspects. Renewable and Sustainable Energy Reviews 56, 1207–1226. doi:10.1016/j.rser.2015.12.014.

Huang, W., Wang, J., Wang, J., Zhou, M., Cao, J., Cai, L., 2024. Capacity optimization of PV and battery storage for EVCS with multi-venues charging behavior difference towards economic targets. Energy 313, 133833. doi:10.1016/j.energy.2024.133833.

Huang, X., Wu, D., Boulet, B., 2023. MetaProbformer for Charging Load Probabilistic Forecasting of Electric Vehicle Charging Stations. IEEE Transactions on Intelligent Transportation Systems 24, 10445–10455. doi:10.1109/TITS.2023.3276947.

Hull, C., Wust, J., Booysen, M., McCulloch, M., 2024. Techno-economic optimization and assessment of solar-battery charging station under grid constraints with varying levels of fleet EV penetration. Applied Energy 374, 123990. doi:10.1016/j.apenergy.2024.123990.

Hüttel, F.B., Peled, I., Rodrigues, F., Pereira, F.C., 2021. Deep Spatio-Temporal Forecasting of Electrical Vehicle Charging Demand. doi:10.48550/ARXIV.2106.10940. version Number: 1.

Ibrahim, R.A., Gaber, I.M., Zakzouk, N.E., 2024. Analysis of multidimensional impacts of electric vehicles penetration in distribution networks. Scientific Reports 14, 27854. doi:10.1038/s41598-024-77662-6.

Ji, N., Zhu, R., Huang, Z., You, L., 2024. An urban-scale spatiotemporal optimization of rooftop photovoltaic charging of electric vehicles. Urban Informatics 3, 4. doi:10.1007/s44212-023-00031-7.

Jian, L., Yongqiang, Z., Hyoungmi, K., 2018. The potential and economics of EV smart charging: A case study in Shanghai. Energy Policy 119, 206–214. doi:10.1016/j.enpol.2018.04.037.

Jones, C.B., Lave, M., Vining, W., Garcia, B.M., 2021. Uncontrolled Electric Vehicle Charging Impacts on Distribution Electric Power Systems with Primarily Residential, Commercial or Industrial Loads. Energies 14, 1688. doi:10.3390/en14061688.

Jung, F., Schröder, M., Timme, M., 2023. Exponential adoption of battery electric cars. PloS One 18, e0295692. doi:10.1371/journal.pone.0295692.

Kara, E.C., Macdonald, J.S., Black, D., Bérges, M., Hug, G., Kiliccote, S., 2015. Estimating the benefits of electric vehicle smart charging at non-residential locations: A data-driven approach. Applied Energy 155, 515–525. doi:10.1016/j.apenergy.2015.05.072.

Karuppiah, N., Mounica, P., Balachandran, P.K., Muniraj, R., 2024. Critical review on electric vehicles: chargers, charging techniques, and standards, in: Renewable Energy for Plug-In Electric Vehicles. Elsevier, pp. 81–94. doi:10.1016/B978-0-443-28955-2.00006-8.

Kazemtarghi, A., Mallik, A., Chen, Y., 2024. Dynamic pricing strategy for electric vehicle charging stations to distribute the congestion and maximize the revenue. International Journal of Electrical Power & Energy Systems 158, 109946. doi:10.1016/j.ijepes.2024.109946.

Khalid, M., Thakur, J., Mothilal Bhagavathy, S., Topel, M., 2024. Impact of public and residential smart EV charging on distribution power grid equipped with storage. Sustainable Cities and Society 104, 105272. doi:10.1016/j.scs.2024.105272.

Khalife, A., Fay, T.A., Göhlich, D., 2022. Optimizing Public Charging: An Integrated Approach Based on GIS and Multi-Criteria Decision Analysis. World Electric Vehicle Journal 13, 131. doi:10.3390/wevj13080131.

Khan, T.A., Abdullah-Al-Nahid, S., Tasnim, S., Taseen, M.A., Jamal, T., Aziz, T., 2024. Empowering E-mobility: Day-ahead dynamic time of use tariff for electric vehicle charging. Energy Reports 12, 3218–3242. doi:10.1016/j.egyr.2024.08.086.

Khan, W., Ahmad, F., Alam, M.S., 2019. Fast EV charging station integration with grid ensuring optimal and quality power exchange. Engineering Science and Technology, an International Journal 22, 143–152. doi:10.1016/j.jestch.2018.08.005.

Kim, Y., Kim, S., 2021. Forecasting Charging Demand of Electric Vehicles Using Time-Series Models. Energies 14, 1487. doi:10.3390/en14051487.

Koohfar, S., Woldemariam, W., Kumar, A., 2023. Prediction of Electric Vehicles Charging Demand: A Transformer-Based Deep Learning Approach. Sustainability 15, 2105. doi:10.3390/su15032105.

Kuehnel, N., Rewald, H., Axer, S., Zwick, F., Findeisen, R., 2022. Flow-inflated selective sampling: Efficient agent-based dynamic ride-sharing simulations , 22 p.doi:10.3929/ETHZ-B-000569127. artwork Size: 22 p. Medium: application/pdf Publisher: ETH Zurich.

Kumar, D.S., Sharma, A., Arphaphiphatphong, V., Mervyn, L., Jie, N., Yi, N., Srinivasan, D., 2021. Power Quality Assessment of Electric Vehicles on the Distribution Networks, in: 2021 IEEE PES Innovative Smart Grid Technologies - Asia (ISGT Asia), IEEE, Brisbane, Australia. pp. 1–5. doi:10.1109/ISGTAsia49270.2021.9715630.

Lee, C., Han, J., 2017. Benders-and-Price approach for electric vehicle charging station location problem under probabilistic travel range. Transportation Research Part B: Methodological 106, 130–152. doi:10.1016/j.trb.2017.10.011.

Li, J., Wang, G., Wang, X., Du, Y., 2023. Smart charging strategy for electric vehicles based on marginal carbon emission factors and time-of-use price. Sustainable Cities and Society 96, 104708. doi:10.1016/j.scs.2023.104708.

Lin, W., Wei, H., Yang, L., Zhao, X., 2024. Technical review of electric vehicle charging distribution models with considering driver behaviors impacts. Journal of Traffic and Transportation Engineering (English Edition) 11, 643–666. doi:10.1016/j.jtte.2024.06.001.

Liu, G., Chinthavali, M.S., Debnath, S., Tomsovic, K., 2021. Optimal m sizing of an electric vehicle charging station with integration of pv and energy storage, in: 2021 IEEE Power & Energy Society Innovative Smart Grid Technologies Conference (ISGT), IEEE, Washington, DC, USA. pp. 1–5. doi:10.1109/ISGT49243.2021.9372269.

Liu, Z., Du, Y., 2023. Evolution towards dispatchable PV using forecasting, storage, and curtailment: A review. Electric Power Systems Research 223, 109554. doi:10.1016/j.epsr.2023.109554.

Lou, J., Shen, X., Niemeier, D.A., Hultman, N., 2024. Income and racial disparity in household publicly available electric vehicle infrastructure accessibility. Nature Communications 15, 5106. doi:10.1038/s41467-024-49481-w.

Lund, H., Münster, E., Tambjerg, L.H., 2004. EnergyPlan: computer model for energy system analysis version 6.0. Division of Technology, Environment and Society, Department of Development and Planning, Aalborg University, Aalborg. OCLC: 783736595.

Lund, H., Thellufsen, J.Z., 2022. EnergyPLAN - Advanced Energy Systems Analysis Computer Model doi:10.5281/ZENODO.4001540. publisher: Zenodo Version Number: 16.2.

Maity, A., Sarkar, S., 2023. Data-Driven Probabilistic Energy Consumption Estimation for Battery Electric Vehicles with Model Uncertainty. doi:10.48550/arXiv.2307.00469. arXiv:2307.00469 [cs].

Menter, J., Fay, T.A., Grahle, A., Göhlich, D., 2023. Long-Distance Electric Truck Traffic: Analysis, Modeling and Designing a Demand-Oriented Charging Network for Germany. World Electric Vehicle Journal 14, 205. doi:10.3390/wevj14080205.

Meyers, A., Yang, H., 2022. Markov Chains for Fault-Tolerance Modeling of Stochastic Networks. IEEE Transactions on Automation Science and Engineering 19, 2591–2606. doi:10.1109/TASE.2021.3093035.

Muratori, M., Jadun, P., Bush, B., Hoehne, C., Vimmerstedt, L., Yip, A., Gonder, J., Winkler, E., Gearhart, C., Arent, D., 2021. Exploring the future energy-mobility nexus: The transportation energy & mobility pathway options (TEMPO) model. Transportation Research Part D: Transport and Environment 98, 102967. doi:10.1016/j.trd.2021.102967.

Nanda, V.M.V., Tateosian, L., Baran, P., 2020. GIS-Based Estimation of Seasonal Solar Energy Potential for Parking Lots and Roads, in: 2020 IEEE Green Technologies Conference(GreenTech), IEEE, Oklahoma City, OK, USA. pp. 136–141. doi:10.1109/GreenTech46478.2020.9289801.

Niu, Z., An, K., Ma, W., 2024. Vehicle-to-grid enabled charging infrastructure planning and operations considering demand uncertainties. Transportation Research Part D: Transport and Environment 127, 103918. doi:10.1016/j.trd.2023.103918.

Novosel, T., Perković, L., Ban, M., Keko, H., Pukšec, T., Krajačić, G., Duić, N., 2015. Agent based modelling and energy planning – Utilization of MATSim for transport energy demand modelling. Energy 92, 466–475. doi:10.1016/j.energy.2015.05.091.

Nugraha, S.D., Ashari, M., Riawan, D.C., 2023. Minimizing Power Loss in Distribution Networks by placing Electric Vehicle Charging Stations using Particle Swarm Optimization, in: 2023 International Electronics Symposium (IES), IEEE, Denpasar, Indonesia. pp. 38–43. doi:10.1109/IES59143.2023.10242490.

Parishwad, O., Jia, R., 2023. Prospects of the Activity-Based Modelling Approach: A Review of Sweden's Transport Model- SAMPERS, in: Smart Transportation Systems 2023. Springer Nature Singapore, Singapore. volume 356, pp. 139–148. doi:10.1007/978-981-99-3284-9_13.

Parishwad, O., Jiang, S., Gao, K., 2023. Investigating machine learning for simulating urban transport patterns: A comparison with traditional macro-models. Multimodal Transportation 2, 100085. doi:10.1016/j.multra.2023.100085.

Pilotti, L., Moretti, L., Martelli, E., Manzolini, G., 2023. Optimal E-fleet charging station design with V2G capability. Sustainable Energy, Grids and Networks 36, 101220. doi:10.1016/j.segan.2023.101220.

Polat, H., Hosseinabadi, F., Hasan, M.M., Chakraborty, S., Geury, T., El Baghdadi, M., Wilkins, S., Hegazy, O., 2023. A Review of DC Fast Chargers with BESS for Electric Vehicles: Topology, Battery, Reliability Oriented Control and Cooling Perspectives. Batteries 9, 121. doi:10.3390/batteries9020121.

Potoglou, D., Song, R., Santos, G., 2023. Public charging choices of electric vehicle users: A review and conceptual framework. Transportation Research Part D: Transport and Environment 121, 103824. doi:10.1016/j.trd.2023.103824.

Radermecker, V., Vanhaverbeke, L., 2023. Estimation of Public Charging Demand Using Cellphone Data and Points of Interest-Based Segmentation. World Electric Vehicle Journal 14, 35. doi:10.3390/wevj14020035.

Rietmann, N., Hügler, B., Lieven, T., 2020. Forecasting the trajectory of electric vehicle sales and the consequences for worldwide CO2 emissions. Journal of Cleaner Production 261, 121038. doi:10.1016/j.jclepro.2020.121038.

Rodrigues, R., Pietzcker, R., Sitarz, J., Merfort, A., Hasse, R., Hoppe, J., Pehl, M., Ershad, A.M., Baumstark, L., Luderer, G., 2023. 2040 greenhouse gas reduction targets and energy transitions in line with the EU Green Deal. doi:10.21203/rs.3.rs-3192471/v1.

Sanami, S., Mosalli, H., Yang, Y., Yeh, H.G., Aghdam, A.G., 2025. Demand Forecasting for Electric Vehicle Charging Stations using Multivariate Time-Series Analysis. doi:10.48550/ARXIV.2502.16365. version Number: 1.

Sander, L., Schindler, D., Jung, C., 2024. Application of Satellite Data for Estimating Rooftop Solar Photovoltaic Potential. Remote Sensing 16, 2205. doi:10.3390/rs16122205.

Sayarshad, H.R., 2024. Optimization of electric charging infrastructure: integrated model for routing and charging coordination with power-aware operations. npj Sustainable Mobility and Transport 1, 4. doi:10.1038/s44333-024-00004-6.

Sevdari, K., Calearo, L., Bakken, B.H., Andersen, P.B., Marinelli, M., 2023. Experimental validation of onboard electric vehicle chargers to improve the efficiency of smart charging operation. Sustainable Energy Technologies and Assessments 60, 103512. doi:10.1016/j.seta.2023.103512.

Shi, D., Zhao, J., Wang, Z., Zhao, H., Wang, J., Lian, Y., Burke, A.F., 2023. Spatial-Temporal Self-Attention Transformer Networks for Battery State of Charge Estimation. Electronics 12, 2598. doi:10.3390/electronics12122598.

Shukla, A., Verma, K., Kumar, R., 2019. Impact of EV fast charging station on distribution system embedded with wind generation. The Journal of Engineering 2019, 4692–4697. doi:10.1049/joe.2018.9322.

Sike, W., Liansong, Y., Bo, P., Xiaohu, Z., Peng, C., Yang, S., 2023. Electric Vehicle Charging Load Time-Series Prediction Based on Broad Learning System, in: 2023 IEEE 6th International Conference on Industrial Cyber-Physical Systems (ICPS), IEEE, Wuhan, China. pp. 1–5. doi:10.1109/ICPS58381.2023.10128054.

Singh, S., Vaidya, B., Mouftah, H.T., 2022. Smart EV Charging Strategies Based on Charging Behavior. Frontiers in Energy Research 10, 773440. doi:10.3389/fenrg.2022.773440.

Sreekumar, A., Lekshmi, R., 2024. Electric vehicle charging station demand prediction model deploying data slotting. Results in Engineering 24, 103095. doi:10.1016/j.rineng.2024.103095.

Stecca, M., Vermeer, W., Soeiro, T.B., Ramirez Elizondo, L., Bauer, P., Palensky, P., 2022. Battery Storage Integration in EV Fast Charging Station for Increasing its Revenues and Reducing the Grid Impact, in: 2022 IEEE Transportation Electrification Conference & Expo (ITEC), IEEE, Anaheim, CA, USA. pp. 109–113. doi:10.1109/ITEC53557.2022.9814040.

Thunuguntla, V.K., Maineni, V., Injeti, S.K., Kumar, P.P., Nuvvula, R.S.S., Dhanamjayulu, C., Rahaman, M., Khan, B., 2024. A TOPSIS based multi-objective optimal deployment of solar PV and BESS units in power distribution system electric vehicles load demand. Scientific Reports 14, 29688. doi:10.1038/s41598-024-79519-4.

Tozluoğlu, , Dhamal, S., Yeh, S., Sprei, F., Liao, Y., Marathe, M., Barrett, C.L., Dubhashi, D., 2023. A synthetic population of Sweden: datasets of agents, households, and activity-travel patterns. Data in Brief 48, 109209. doi:10.1016/j.dib.2023.109209.

Vansola, B., Chandra, M., Shukla, R.N., 2023. GIS-Based Model for Optimum Location of Electric Vehicle Charging Stations, in: Recent Advances in Transportation Systems Engineering and Management. Springer Nature Singapore, Singapore. volume 261, pp. 113–126. doi:10.1007/978-981-19-2273-2_8.

Vazifeh, M.M., Zhang, H., Santi, P., Ratti, C., 2019. Optimizing the deployment of electric vehicle charging stations using pervasive mobility data. Transportation Research Part A: Policy and Practice 121, 75–91. doi:10.1016/j.tra.2019.01.002.

Visaria, A.A., Jensen, A.F., Thorhauge, M., Mabit, S.E., 2022. User preferences for EV charging, pricing schemes, and charging infrastructure. Transportation Research Part A: Policy and Practice 165, 120–143. doi:10.1016/j.tra.2022.08.013.

Wang, S., Chen, A., Wang, P., Zhuge, C., 2023. Predicting electric vehicle charging demand using a heterogeneous spatio-temporal graph convolutional network. Transportation Research Part C: Emerging Technologies 153, 104205. doi:10.1016/j.trc.2023.104205.

Westin, K., Jansson, J., Nordlund, A., 2018. The importance of sociodemographic characteristics, geographic setting, and attitudes for adoption of electric vehicles in Sweden. Travel Behaviour and Society 13, 118–127. doi:10.1016/j.tbs.2018.07.004.

Wongsunopparat, S., Cherian, P., 2023. Study of Factors Influencing Consumers to adopt EVs (Electric Vehicles). Business and Economic Research 13, 155. doi:10.5296/ber.v13i2.21054.

Wu, Y., Lu, Y., Zhu, Z., Holguín-Veras, J., 2023. Optimizing Electric Vehicle Charging Infrastructure on Highways: A Multi-Agent-Based Planning Approach. Sustainability 15, 13634. doi:10.3390/su151813634.

Xu, M., Meng, Q., Liu, K., Yamamoto, T., 2017. Joint charging mode and location choice model for battery electric vehicle users. Transportation Research Part B: Methodological 103, 68–86. doi:10.1016/j.trb.2017.03.004.

Xu, Y., Çolak, S., Kara, E.C., Moura, S.J., González, M.C., 2018. Planning for electric vehicle needs by coupling charging profiles with urban mobility. Nature Energy 3, 484–493. doi:10.1038/s41560-018-0136-x.

Yang, S.Y., Woo, J., Lee, W., 2024. Assessing optimized time-of-use pricing for electric vehicle charging in deep vehicle-grid integration system. Energy Economics 138, 107852. doi:10.1016/j.eneco.2024.107852.

Yang, X., Peng, Z., Wang, P., Zhuge, C., 2023. Seasonal variance in electric vehicle charging demand and its impacts on infrastructure deployment: A big data approach. Energy 280, 128230. doi:10.1016/j.energy.2023.128230.

Yao, C., Chen, S., Salazar, M., Yang, Z., 2023. Joint Routing and Charging Problem of Electric Vehicles With Incentive-Aware Customers Considering Spatio-Temporal Charging Prices. IEEE Transactions on Intelligent Transportation Systems 24, 12215–12226. doi:10.1109/TITS.2023.3286952.

Yi, Z., Chen, B., Liu, X.C., Wei, R., Chen, J., Chen, Z., 2023. An agent-based modeling approach for public charging demand estimation and charging station location optimization at urban scale. Computers, Environment and Urban Systems 101, 101949. doi:10.1016/j.compenvurbsys.2023.101949.

Yi, Z., Liu, X.C., Wei, R., Chen, X., Dai, J., 2022. Electric vehicle charging demand forecasting using deep learning model. Journal of Intelligent Transportation Systems 26, 690–703. doi:10.1080/15472450.2021.1966627.

Zaino, R., Ahmed, V., Alhammadi, A.M., Alghoush, M., 2024. Electric Vehicle Adoption: A Comprehensive Systematic Review of Technological, Environmental, Organizational and Policy Impacts. World Electric Vehicle Journal 15, 375. doi:10.3390/wevj15080375.

Zanvettor, G.G., Fochesato, M., Casini, M., Lygeros, J., Vicino, A., 2024. A stochastic approach for EV charging stations in demand response programs. Applied Energy 373, 123862. doi:10.1016/j.apenergy.2024.123862.

Zhong, L., Zeng, Z., Huang, Z., Shi, X., Bie, Y., 2024a. Joint optimization of electric bus charging and energy storage system scheduling. Frontiers of Engineering Management 11, 676–696. doi:10.1007/s42524-024-3102-2.

Zhong, S., Che, Y., Zhang, S., 2024b. Electric Vehicle Charging Load Optimization Strategy Based on Dynamic Time-of-Use Tariff. Energy Engineering 121, 603–618. doi:10.32604/ee.2023.044667.

Zhong, Z., Zeng, Y., Zhao, X., Zhang, S., 2024c. The social benefits resulting from electric vehicle smart charging balancing economy and decarbonization. Transport Policy 147, 113–124. doi:10.1016/j.tranpol.2023.12.020.

Zhuge, C., Bithell, M., Shao, C., Li, X., Gao, J., 2021. An improvement in MATSim computing time for large-scale travel behaviour microsimulation. Transportation 48, 193–214. doi:10.1007/s11116-019-10048-0.

Çelik, S., Ok, , 2024. Electric vehicle charging stations: Model, algorithm, simulation, location, and capacity planning. Heliyon 10, e29153. doi:10.1016/j.heliyon.2024.e29153.

Šolić, A.J., Jakus, D., Vasilj, J., Jolevski, D., 2023. Electric Vehicle Charging Station Power Supply Optimization with V2X Capabilities Based on Mixed-Integer Linear Programming. Sustainability 15, 16073. doi:10.3390/su152216073.

Part I

Appended Publications

Paper I

The Role of Renewable Energy to Promote Future Electric Transport and Power Systems

O. Parishwad, A. Najafi, X. Liu, K. Gao (2025)

The Routledge Handbook of Sustainable Urban Transport (pp. 361-373)

doi:10.4324/9781003425489-30

Paper II

Integrated and agent-based charging demand estimation considering cost-aware and adaptive charging behavior

O. Parishwad, K. Gao, A. Najafi

Submitted to Transportation Research Part D: Transport and Environment,
(under review)

Paper III

Joint optimization of charging infrastructure and renewable energies with battery storage considering user redirection incentives

O. Parishwad, A. Najafi, K. Gao